The Coordination Chemistry of the Pentadentate 2,2,6,6-Tetrakis(aminomethyl)-4-azaheptane (ditame)

Kaspar Hegetschweiler,*[a] Oliver Maas,[a] Anja Zimmer,[a] Rodney J. Geue,[b] Alan M. Sargeson,[b] Jeffrey Harmer,[c] Arthur Schweiger,[c] Irmgard Buder,[d] Günter Schwitzgebel,[d] Vera Reiland,[e] and Walter Frank[e]

Dedicated to Professor Walter Schneider on the occasion of his 75th birthday

Keywords: Amine ligands / Chelates / Ligand design / Stability constants

The protonation and metal complex formation of the branched pentaamine ligand 2,2,6,6-tetrakis(aminomethyl)-4-azaheptane (ditame, L) with Co^{II}, Co^{III}, Ni^{II}, Cu^{II}, Zn^{II}, and Cd^{II} have been studied. The crystal structures of $[Ni(ditame)(EtOH)]Br_2$, $[Co_2(ditame)_2(O_2)]Cl_4{\cdot}4H_2O$, and $[Co_2(ditame)_2(O_2)]Cl_2[ZnCl_4][ZnCl_3(H_2O)]{\cdot}H_2O$ were determined by X-ray diffraction analyses. The metal complexes showed octahedral coordination geometries with exclusive formation of six-membered chelate rings, the four primary amino groups being in equatorial positions and the secondary amino group (N^{sec}) apical. This geometry enforces a relatively short M–N^{sec} bond. Complex formation in aqueous solution was evaluated by potentiometric titration. The ditame ligand forms a surprisingly stable Ni^{II} complex with $\log K_{NiL} = 17.8$ (25 °C, 0.1 M KNO_3), and formation of protonated species $[Ni(H_n ditame)]^{(n+2)+}$ (n = 1, 2) is not significant. Different behavior is evident for Zn^{II} and Cd^{II}, with which protonated species are extensively formed, while the stability of $[ML]^{2+}$ is relatively low. Complex formation between ditame and Cu^{II} in the range $3 < pH < 7$ resulted in the formation of $[Cu(H_2ditame)]^{4+}$. In slightly alkaline solution, the dinuclear $[Cu_2(ditame)_2]^{4+}$ appears to be formed. The structural assignment of this dimer is based on its UV/Vis and EPR characteristics, with the EPR data indicating a $Cu^{II}\cdots Cu^{II}$ separation of about 5.9 Å. The redox behavior of the Ni and Co complexes was investigated by cyclic voltammetry. The mononuclear species showed quasi-reversible electron transfer for the $Ni^{II/III}$ and $Co^{II/III}$ couples. For the dinuclear peroxo/superoxo-bridged Co^{III} complexes, quasi-reversible electron transfer corresponding to oxidation/reduction of the O_2^{2-}/O_2^- bridge was observed.

Introduction

Ligand design is a well-established field in modern coordination chemistry.[1] Tailored complexing agents are of importance for the construction of catalysts,[2] and as building blocks for coordination polymers,[3,4] since they allow specific modulation of the electronic and steric properties of a metal complex.[5] Pentadentate chelators are of particular interest, since the high denticity often gives rise to high stability, while the binding of an additional ligand (e.g. a substrate) to the metal cation within an octahedral environment is still possible.[6–16] As regards complex formation with late transition metal cations, aliphatic polyamines are of particular relevance.[17,18] Various aliphatic and alicyclic pentaamines have been prepared and their coordination chemistry explored. They comprise a series of pentaaza macrocycles[19] as well as tetraaza and triaza macrocycles with pendant amine groups.[20] Macrobicyclic pentaaza ligands are also known,[19] and a number of open-chain, linear, and branched aliphatic pentaamines have been described.[6,7,21–25] The synthesis of the doubly branched 2,2,6,6-tetrakis(aminomethyl)-4-azaheptane, or ditame (Scheme 1), has recently been reported by some of us, and the structure and reactivity of its Co^{III} complex have been discussed in detail.[21] Metal complex formation by a related pyridine analogue has been published by Grohmann and

[a] Anorganische Chemie, Universität des Saarlandes
Postfach 15 11 50, 66041 Saarbrücken, Germany
Fax: (internat.) + 49-681/302-2663
E-mail: hegetschweiler@mx.uni-saarland.de
[b] Research School of Chemistry, Australian National University, Canberra, ACT 0200, Australia
[c] Laboratorium für Physikalische Chemie, ETH Hönggerberg, 8093 Zürich, Switzerland
[d] Physikalische Chemie, Universität des Saarlandes
Postfach 15 11 50, 66041 Saarbrücken, Germany
[e] Institut für Anorganische Chemie und Strukturchemie, Heinrich-Heine-Universität Düsseldorf,
Universitätsstr. 1, 40225 Düsseldorf, Germany
Supporting information for this article is available on the WWW under http://www.eurjic.org or from the author.

co-workers.[10−16] This investigation explores the stability of labile coordination complexes of ditame in comparison with the coordination chemistry of two related hexadentate ligands (Scheme 1), 1,1,1-tris(5-amino-2-azapentyl)ethane (stn) and 1,1,1-tris(4-amino-2-azabutyl)ethane (sen).[26]

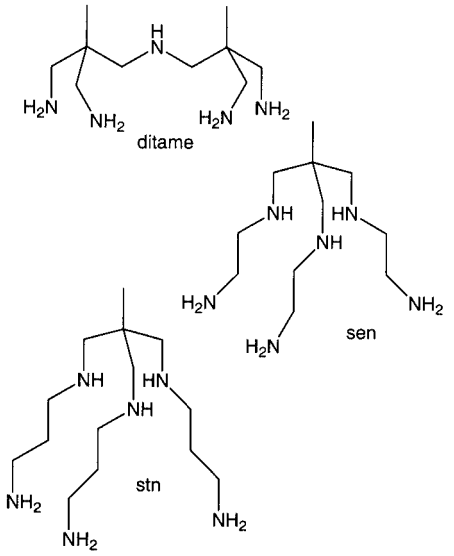

Scheme 1

Results and Discussion

Protonation of ditame

Because of the fairly high charges of multiply protonated amines, increased electrostatic effects have to be taken into account. It is known that some cyclic, multiply protonated polyamines selectively bind suitable anions such as chloride or nitrate through hydrogen bonding.[19] Such interactions could influence the acidity constants of the ligand. Since precise pK_a values of the ligand are a prerequisite for conclusive analysis of metal complex formation in aqueous solution, a series of pK_a determinations was performed, with the nature and concentration of the inert electrolyte (KCl and KNO_3, 0.1 and 1.0 M) as well as the total concentration of ditame (1−10 mM) being varied. Inspection of the corresponding values (Table 1) reveals a significant dependence of the pK_a values on the ionic strength. The acidities of multiply protonated species decrease at higher salt concentrations, and this effect increases with increasing degree of protonation.[27] The effect of the anion (Cl^- versus NO_3^-) was negligible, so specific binding of these anions by the open-chained H_xL^{x+} appears not to be significant in aqueous solution. However, a weak but significant dependence of the pK_a values on total ligand concentration is evident, indicating some deviation from ideal behavior for solutions in which the ratio of total ditame to the ionic strength exceeds a value of 1:500.

Table 1. pK_a values of ditame (25 °C) for different inert electrolytes

Ionic strength [M]	0.1	0.1	1.0	1.0	1.0
Inert electrolyte	KCl	KNO_3	KCl	KCl	KNO_3
Total L [M]	0.001	0.001	0.002	0.010	0.010
p$K_{a,1}$[a]	–[b]	–[b]	1.7(1)	1.8(1)	1.8(1)
p$K_{a,2}$	6.77	6.83	7.32	7.36	7.40
p$K_{a,3}$	7.90	7.90	8.26	8.32	8.33
p$K_{a,4}$	9.47	9.44	9.61	9.72	9.76
p$K_{a,5}$	11.10	11.09	11.06	11.25	11.28

[a] $pK_{a,i} = -\log K_{a,i}$, $K_{a,i} = [H_{5-i}L] \times [H] \times [H_{6-i}L]^{-1}$, estimated standard deviations are 0.01 or less unless otherwise noted. [b] Value too low for determination by pH-metric methods.

A series of pD-dependent ^1H NMR spectra were measured in D_2O (Figure 1). These exhibit four signals for the H(−C) protons of the C_{2v}-symmetric[21] H_xL^{x+} entity, a singlet for the two homotopic methyl groups (X), an additional singlet (Y) for the enantiotopic methylene protons [$H^{(Y1)}$ and $H^{(Y2)}$], and an AB system for the diastereotopic protons $H^{(Za)}$ and $H^{(Zb)}$ of the four methylene groups (Z). Since the chemical shifts of $H^{(Za)}$ and $H^{(Zb)}$ differ only slightly over the entire pD range, a mean value corresponding to the center of the AB system (Z) is presented in Figure 1. The pD-dependence of these signals was modeled by minimization of $\Sigma(\delta_{obs} - \delta_{calc})^2$, assuming a rapid equilibrium with weighted averaged shifts (δ_{obs}) for the six macrospecies H_xL^{x+} ($0 \le x \le 5$, see Table S1).[28,29] The resulting pK_a values of 0.9, 7.2, 8.0, 9.3, and 11.0 agree well with the values obtained from potentiometric titrations. In the fully protonated and the fully deprotonated forms, the two types of methylene groups (Y and Z) have rather similar environments, with similar chemical shifts. For some of the intermediate forms H_xL^{x+} ($2 \le x \le 4$), however, the chemical shifts of Y and Z differ significantly. This observation is attributed to different tautomeric forms that have to be taken into account for the partially protonated species, with the secondary nitrogen atom either protonated or not protonated. Additionally, the four primary amino groups of H_2L^{2+} and H_3L^{3+} can be protonated in different ways, which results in the generation of further tautomers. However, since the four primary amino groups appear to be symmetry-equivalent on the NMR timescale, the latter type of tautomerism can be taken account of by means of an averaged, partial protonation of the NH_2 groups. A total of two microspecies for each of the partially protonated forms is thus sufficient for a suitable description of the NMR characteristics. A set of empirically derived deshielding parameters was used to elucidate the equilibrium between the different microspecies.[28,29] These parameters were determined by use of the well-established observation that protonation of an amino group generally results in a deshielding of nearby H(−C) protons, and that this effect decreases with increasing distance.[30,31] In the range $10 < pD < 12$, the related pD dependence of Y and Z is indicative of fairly unspecific binding of the first proton. The quantit-

ative analysis suggests 25% protonation at the secondary amino group in HL^+, approximately corresponding to a statistical distribution of the proton over the five basic sites. Obviously, there is no significant difference in basicity between the secondary and primary nitrogen donors. For H_2L^{2+}, protonation at the secondary nitrogen atom is < 10%, and in H_3L^{3+} and H_4L^{4+} the protons are exclusively bonded to the primary amino groups. Therefore, consecutive protonation of L up to H_4L^{4+} resulted in increasing protonation at the primary amino groups and decreasing protonation at the secondary amino group. Consequently, the chemical shifts of X and Z increase steadily with increasing protonation (Figure 1), whereas the methylene protons Y are less deshielded in H_2L^{2+} than in HL^+. A dramatic deshielding of Y is observed on final protonation of H_4L^{4+}. However, since H_4L^{4+} is a rather weak base, the exclusive presence of the fully protonated H_5L^{5+} is only observed in strongly acidic solutions (pD = 0).

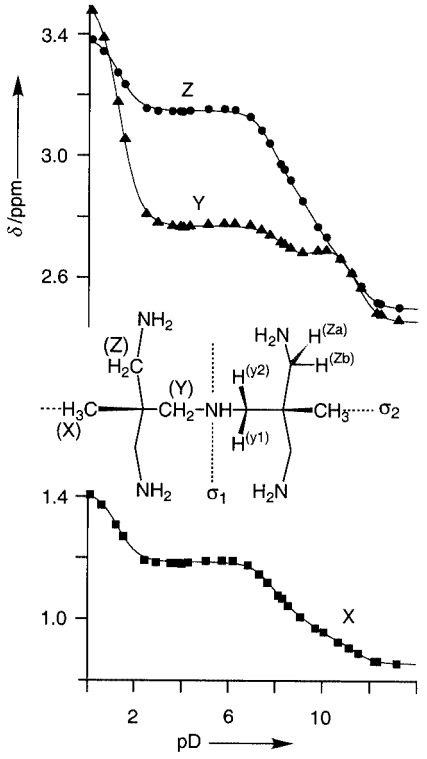

Figure 1. pD dependence of the ^1H NMR resonances of $H_x$ditame^{x+}; the points correspond to experimental values, the lines are calculated (least-squares), by assuming a rapid equilibrium; the values of Z correspond to the center of the AB system of Z^a and Z^b; the schematic formula indicates the observed C_{2v} symmetry with the mirror plane σ_1 and the pseudo mirror plane σ_2[21]

Crystal Structures

[Ni(ditame)(EtOH)]Br$_2$ (1Br$_2$)

The complex cations $\mathbf{1}^{2+}$ and the Br^- anions are arranged in linear chains along the crystallographic *b* axis through $Ni^{II}-N-H\cdots Br^-$ and $Ni^{II}-O-H\cdots Br^-$ hydrogen bonding. Two such chains, related through a crystallographic screw axis, form a double-chain structure. The $\mathbf{1}^{2+}$ cation (Figure 2) is situated on a crystallographic mirror plain, approximately corresponding to the molecular pseudo-plane σ_2 (Figure 1). However, the symmetry operation σ_2 requires either a planar geometry or rapid inversion of the pyramidal configuration for the secondary nitrogen atom. Obviously, neither requirement can be met in the metal complex, and the inherent violation of this symmetry has resulted in a characteristic disorder. The cation was thus refined by two superimposed, but completely independent models (mirror images) with occupancies of 50% each (Figure S1). A similar type of disorder has previously been reported for [Co(ditame)Cl][$ZnCl_4$].[21]

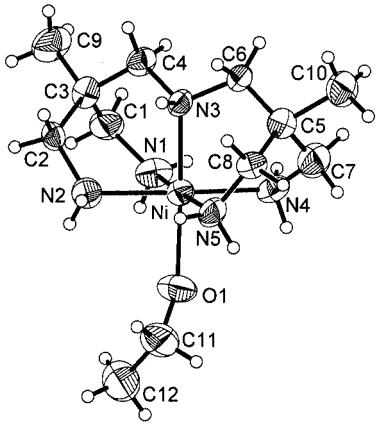

Figure 2. Molecular structure of $[Ni(ditame)(EtOH)]^{2+}$ ($\mathbf{1}^{2+}$); the atomic displacement ellipsoids are drawn at the 50% probability level; hydrogen atoms are shown as spheres of arbitrary size; selected bond lengths [A] and angles [°]: Ni−N1 2.111(7), Ni−N2 2.107(7), Ni−N3 2.050(5), Ni−N4 2.115(7), Ni−N5 2.113(7), Ni−O1 2.172(6); N1−Ni−N2 85.0(3), N1−Ni−N3 93.2(3), N1−Ni−N4 92.4(4), N1−Ni−N5 176.9(4), N1−Ni−O1 86.8(3), N2−Ni−N3 86.8(3), N2−Ni−N4 177.1(3), N2−Ni−N5 98.1(4), N2−Ni−O1 90.2(3), N3−Ni−N4 92.2(3), N3−Ni−N5 87.2(2), N3−Ni−O1 177.0(3), N4−Ni−N5 84.6(3), N4−Ni−O1 90.8(3), N5−Ni−O1 92.9(3)

[Co$_2$(ditame)$_2$(O$_2$)]Cl$_4$·4H$_2$O (2Cl$_4$·4H$_2$O)

The Co−O−O−Co group of the peroxo complex $\mathbf{2}^{4+}$ was located on a twofold rotational axis. It could be refined without problems, although considerable anisotropy for the atomic displacement of the primary nitrogen atoms indicated some conformational disorder within the ditame moieties (Figure 3). The dimeric cation $\mathbf{2}^{4+}$ and the counterions again form a chain structure. The chains are oriented parallel to *b* and coincide with the twofold rotational axes, forming a type of distorted hexagonal rod packing.

[Co$_2$(ditame)$_2$(O$_2$)]Cl$_2$[ZnCl$_4$][ZnCl$_3$(H$_2$O)]·H$_2$O {3Cl$_2$[ZnCl$_4$][ZnCl$_3$(H$_2$O)]·H$_2$O}

The centrosymmetric superoxo complex $\mathbf{3}^{5+}$ (Figure 4) was located and refined without problems, although the counter-ion and the water of crystallization showed some disorder. The positive charge of +2.5 in the asymmetric

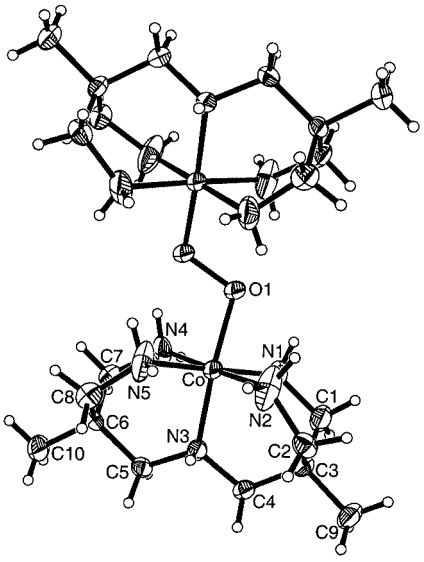

Figure 3. Molecular structure of $[Co_2(ditame)_2O_2]^{4+}$ ($\mathbf{2}^{4+}$); the atomic displacement ellipsoids are drawn at the 50% probability level; hydrogen atoms are shown as spheres of arbitrary size; selected bond lengths [Å] and angles [°]: Co−N1 1.987(8), Co−N2 1.950(8), Co−N3 1.920(7), Co−N4 1.973(8), Co−N5 1.978(8), Co−O1 1.951(7), O1−O1′ 1.495(11); N1−Co−N2 86.7(4), N1−Co−N3 92.7(4), N1−Co−N4 92.8(5), N1−Co−N5 177.6(6), N1−Co−O1 79.8(4), N2−Co−N3 88.1(5), N2−Co−N4 177.9(6), N2−Co−N5 95.4(5), N2−Co−O1 93.8(5), N3−Co−N4 93.9(4), N3−Co−N5 88.5(5), N3−Co−O1 172.1(5), N4−Co−N5 85.1(4), N4−Co−O1 84.1(4), N5−Co−O1 98.9(4), O1′−O1−Co: 110.4(5)

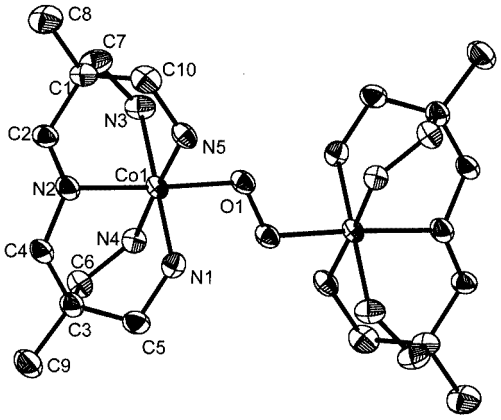

Figure 4. Molecular structure of $[Co_2(ditame)_2O_2]^{5+}$ ($\mathbf{3}^{5+}$); the atomic displacement ellipsoids are drawn at the 50% probability level; hydrogen atoms are omitted for clarity; selected bond lengths [Å] and angles [°] Co−N1 1.956(6), Co−N2 1.949(6), Co−N3 1.963(6), Co−N4 1.966(6), Co−N5 1.970(6), Co−O1 1.917(5), O1−O1′ 1.341(10); N1−Co−N2 91.6(3), N1−Co−N3 176.9(3), N1−Co−N4 88.6(3), N1−Co−N5 90.3(3), N1−Co−O1 92.8(2), N2−Co−N3 87.5(3), N2−Co−N4 88.1(3), N2−Co−N5 94.5(3), N2−Co−O1 175.4(2), N3−Co−N4 94.3(3), N3−Co−N5 86.8(3), N3−Co−O1 88.1(2), N4−Co−N5 177.2(3), N4−Co−O1 90.8(2), N5−Co−O1 86.7(2), O1′−O1−Co 116.0(5)

unit is balanced by a Cl^- anion and an additional tetrahedral ZnX_4 moiety. Three of these X positions could be unambiguously refined as Cl atoms; the fourth position exhibited two maxima in an electron density map with a separation of 0.69(2) Å. These two positions were refined as a Cl and an O atom, each with 50% occupancy. The corresponding distances to the Zn center, of 2.28(1) and 2.08(3) Å, are in agreement with a Zn−Cl and a Zn−OH_2 bond, respectively.[32,33] Obviously, the ZnX_4 positions are equally and randomly shared by $[ZnCl_4]^{2-}$ and $[ZnCl_3(OH_2)]^-$ anions; the simultaneous presence of these two anions has frequently been observed in solid-state structures.[33] An additional water molecule, located in proximity to two ZnX_4 moieties, was distributed over three positions with site occupancies of 28−36%. The zincate anions and the water molecule form chains of composition $[ZnCl_4]\cdots H_2O\cdots[ZnCl_3(H_2O)]\cdots$ along the crystallographic *c* axis. Additional chains along *c* were formed by $\mathbf{3}^{5+}$ and the Cl^- counter-ions. They are stabilized by Co−N−H···Cl^- hydrogen bonds.

Molecular Structures of the ditame Complexes

The crystal structures of two mononuclear Co^{III}(ditame) complexes have been reported previously.[21] The structures of $\mathbf{1}^{2+}$ and of the dinuclear $\mathbf{2}^{4+}$ and $\mathbf{3}^{5+}$ (Figures 2−4) each display a closely related coordination mode for the ditame ligand, with exclusive formation of six-membered chelate rings. The four primary nitrogen donors form an almost regular square, with a slight distortion towards an isosceles trapezium: The $N^{prim}\cdots N^{prim}$ distances in one tripodal tris(aminomethyl)ethane (= tame) cap are slightly shorter than corresponding distances between the nitrogen atoms belonging to different caps. Moreover, the inter-tame N···N distances are inequivalent, the N···N distance with a *cisoid* orientation towards the (N^{sec})−H hydrogen is longer than that with a *transoid* orientation. In all three complexes, the M(ditame) moiety exhibits approximate local C_s symmetry, although the corresponding mirror plain (σ_1 in Figure 1) never corresponds to a crystallographic symmetry element. The M−N^{sec} bond is always somewhat shorter than the corresponding bonds to the primary amino groups. This is also the case if a ligand with a significant *trans* influence[34−36] such as O_2^{2-} is bonded *trans* to N^{sec}, and it appears that the short M−N^{sec} bond is a consequence of the steric requirements of this particular ligand.[15]

The Co−O−O−Co structures of $\mathbf{2}^{4+}$ and $\mathbf{3}^{5+}$ exhibited characteristic differences. The O−O lengths of 1.495 and 1.341 Å are indicative of an O_2^{2-} and an O_2^- bridge, respectively. Corresponding distances for related monobridged (pentaamine)Co^{III} complexes are 1.42−1.53 Å for O_2^{2-} and 1.27−1.34 Å for O_2^-.[6−9,15,23,34−43] The presence of a peroxo bridge in $\mathbf{2}^{4+}$ is also indicated by the Raman data, with an O−O stretch vibration at 810 cm^{-1}.[7,15,35,44] The $Co^{III}-O_2^-$ bond of 1.917(5) Å in the superoxo complex $\mathbf{3}^{5+}$ is in good agreement with literature values, but the $Co^{III}-O_2^{2-}$ bond [1.951(7) Å] in $\mathbf{2}^{4+}$ is unusually long (reported range: 1.83−1.92 Å).[6,8,9,15,23,34−39] The Co^{III}−O−O angles and the average Co^{III}−N distances in both complexes are all normal. The superoxo complex $\mathbf{3}^{5+}$ has a planar, *transoid* Co−O−O−Co grouping with a torsional angle τ of 180°, whereas the Co−O−O−Co grouping in the peroxo complex $\mathbf{2}^{4+}$ is twisted with τ = 138.1°. In agreement with our findings, dinuclear, monobridged

Co^{III}(pentaamine)(superoxo) complexes reported to date are centrosymmetric[7,15,40−42] or nearly centrosymmetric[43] ($\tau = 175°$). For (pentaamine)Co^{III}(peroxo) complexes, both planar *transoid*[6,23,34,35,37,38] and bent[8,9,15,36,39] structures have been described, examples with $\tau = 180°$ predominating. The known non-centrosymmetric, bent structures have torsional angles τ of 146−177.5°.[45] Obviously, $\mathbf{2}^{4+}$ exhibits a particularly high degree of such torsional twist. It has been argued that the value of τ is strongly influenced by inter- and intramolecular hydrogen bonding. In particular, hydrogen bonds between the coordinated amino groups and the remote oxygen atom of the peroxo bridge have been proposed to be a major structure-determining factor.[15,23] However, the corresponding $N\cdots O^{remote}$ distances depend on the rotation around the Co−O bond rather than about O−O. A conclusive discussion of the different types of rotamers requires consideration of three torsional angles τ, φ^a, and φ^b (Scheme 2, φ^a and φ^b are defined as the torsional angles $O-O\cdots N^{sec}-H$). The symmetry types of the various conformers can be mapped as functions of these three parameters; *transoid* conformations ($\tau = 180°$) with $\varphi^a = \varphi^b = 180°$ or $\varphi^a = \varphi^b = 0°$ have the highest possible symmetry (C_{2h}).[42] Further *transoid* conformations have C_s ($\varphi^a = 0$, $\varphi^b = 180°$), C_i ($\varphi^a = -\varphi^b$), or C_2 ($\varphi^a = \varphi^b$) symmetry. For $\tau < 180°$ and $\varphi^a = \varphi^b$ the symmetry remains C_2. Evidently, all conformations with $0° < |\varphi^a| \neq |\varphi^b| < 180°$ are completely asymmetric (C_1). The prerequisite for the formation of four equal intramolecular $N-H\cdots O^{remote}$ hydrogen bonds is $|\varphi^a|, |\varphi^b| = 0$, 90, or 180°. Several of the symmetry types described above match these requirements (even C_1). Neither a centrosymmetric structure nor the *transoid* conformation is required.[23]

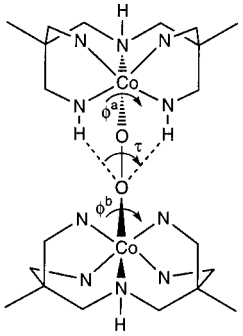

Scheme 2

In the crystal structures reported here, the superoxo and the peroxo complexes have a C_i ($\tau = 180°$, $\varphi^a = 86.2°$, $\varphi^b = -86.2°$) and a C_2 ($\tau = 138.1°$, $\varphi^a = -82.7°$, $\varphi^b = -82.7°$) structure, respectively. Only one strong $N-H\cdots O^{remote}$ hydrogen bond per Co(ditame) moiety is formed in each complex. Since the two Co(ditame) moieties are twisted against each other by an angle of almost 90°, the four methyl groups are not equivalent. In solution (D_2O, pD = 7), however, we observed only one single signal for these methyl groups in the ^1H and the ^{13}C NMR spectra of the peroxo complex $\mathbf{2}^{4+}$. The methylene groups exhibited three AB systems (six unique H atoms) in the ^1H NMR, and the ^{13}C NMR showed a total of five lines. These characteristics are only compatible with a C_{2h} structure. Variation in temperature did not produce any unusual line-broadening effect, and it appears that the barriers of rotation for the Co−O and the O−O bonds are − as would be expected − fairly small. The different values of τ reported in the literature are thus most probably based on the crystal packing and not on any electronic effect.

Evidence of the different conformations of $\mathbf{2}^{4+}$ in solution and in the solid state is also provided by UV/Vis spectroscopy. In solution the typical spectrum of a monobridged, centrosymmetric complex[46−48] with $\lambda_{max} = 296$ nm, $\log \varepsilon = 4.1$ (π_σ* CT), and shoulders around 420 and 520 nm has been observed. In the solid state, an intense CT band remained at about 300 nm, but an additional shoulder appeared at about 380 nm while the 420 and 520 nm bands gained in intensity. This behavior is clearly indicative of the diminished symmetry in the solid state, in which some transitions, symmetry-forbidden in the C_{2h} forms, become allowed. A more detailed discussion on the electronic properties of this complex will be given elsewhere.[49] The spectrum of the superoxo complex $\mathbf{3}^{5+}$ has maxima at 471 nm ($\log \varepsilon = 2.3$) and 695 nm ($\log \varepsilon = 2.9$). These values agree well with the characteristics reported for monobridged Co^{III}(pentaamine)(superoxo) complexes.[7,15,41,42,50]

Complex Formation of ditame (= L) with Co^{II}, Ni^{II}, Zn^{II}, and Cd^{II} in Aqueous Solution

Potentiometric measurements were performed to evaluate complex formation as a function of pH (Figure 5), and to determine the corresponding formation constants (Table 2). For Co^{II}, Ni^{II}, Zn^{II}, and Cd^{II} the predominant species at $8 < pH < 11$ is the 1:1 complex $[ML]^{2+}$. The observed order of stability $Co^{II} < Ni^{II} > Zn^{II}$ is in agreement with the well-established Irving−Williams series.[51] Differences between 0.1 M KNO_3 and 0.1 M KCl are generally small, with the exception of Cd, for which formation of chloro complexes must be taken into account.[28] The difference between Cd^{II} and Zn^{II} ($\Delta\log \beta_{110} = 2.8$ in 0.1 M KNO_3) is fairly large. Such an effect can be attributed to the formation solely of six-membered chelate rings, which is more favorable for the smaller cation.[52] Additional species of composition $[M(HL)]^{3+}$ and $[M(H_2L)]^{4+}$ appeared at lower pH values. Formation of such protonated components is almost negligible for Co^{II} and Ni^{II} but more significant for Zn^{II} and Cd^{II}. In these latter species, the donor set is necessarily only partially bonded to the metal cation, one or two nitrogen atoms of the primary amino groups remaining protonated. In the alkaline range, hydroxo complexes of composition $[ML(OH)]^+$ formed, thus indicating additional coordination of a solvent molecule which can be deprotonated. A corresponding octahedral NiN_5O structure has been established by X-ray analysis (Figure 2) and was confirmed in solution by the Vis spectrum of $[Ni(ditame)(H_2O)]^{2+}$, with bands at 338, 533, and 884 nm.[4] The pK_a values of the $[ML(H_2O)]^{2+}/[ML(OH)]^+$ couples can be calculated as $pK_a = \log \beta_{110} - \log \beta_{11-1}$. For the divalent cations, they

showed only minor differences: 11.7 (Co^{II}), 12.0 (Ni^{II}), 11.8 (Zn^{II}), and 11.7 (Cd^{II}). For the inert Co^{III}, the corresponding value was determined directly by acid-base titration. As was to be expected,[15,17,24] the water molecule bonded to this trivalent cation was considerably more acidic (pK_a = 6.38).

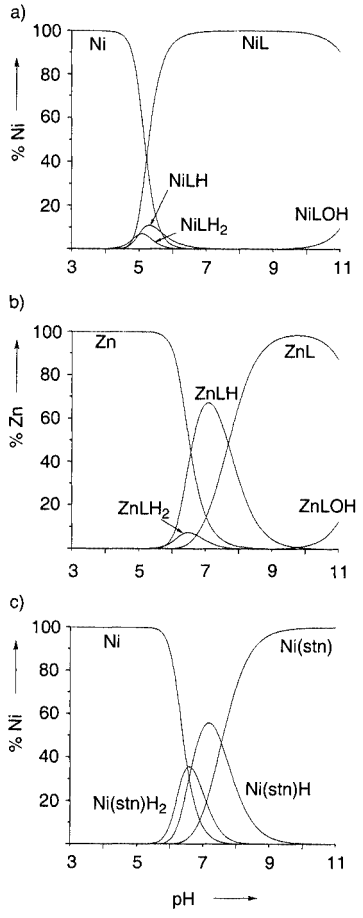

Figure 5. Species distribution plots for equilibrated aqueous solutions; a) Ni^{II} and ditame, b) Zn^{II} and ditame, c) Ni^{II} and stn; total metal and total ligand (L = ditame) concentrations are 1 mM; only metal-containing species are shown; the equilibrium constants listed in Tables 1 and 2 were used for the calculations

Stability constants for metal complexes with representative pentaamine ligands are given in Table 3. These values clearly show that ditame forms a surprisingly stable complex with Ni^{II}. The formation constant of the 1:1 complex has the same order of magnitude as those observed for corresponding complexes with the linear, open-chained tetren or the macrocyclic [16]aneN5. For Zn^{II} and Cd^{II} the situation is different; here the linear and the macrocyclic representatives form 1:1 complexes of higher stability. Obviously, the ditame geometry appears to be particularly suited for the accommodation of relatively small metal ions with a pronounced preference for an octahedral coordination. The particular metal-binding properties of ditame can be elucidated further by comparison with ligands representing different types of substructures with the ditame geometry (Table 4). It is particularly interesting that the addition of two aminomethyl branches to the linear 1,5,9-triazanonane (3,3-tri) ligand at the 3- and the 7-positions increases the stability of the Ni^{II} complex by almost nine orders of magnitude. Again, this effect is much less pronounced for Zn^{II} and Cd^{II}. Similarly, the fusion of two "tame" fragments to the ditame structure is particularly effective for Ni^{II}. Some examples listed in Tables 3 and 4 also support the notion that an increasing number of six-membered chelate rings usually results in a reduction in complex stability. Such destabilization is not observed for ditame, however, although this ligand forms six-membered chelate rings exclusively. The *penta*dentate ditame forms more stable complexes with Co^{II} and Ni^{II}, than the *hexa*dentate stn. This behavior is consistent with the observation that protonated Ni(ditame) complexes are minor species whereas $[Ni(Hstn)]^{3+}$ and $[Ni(H_2stn)]^{4+}$ are substantial components in neutral solution (Figure 5). Even the sen ligand, with three five-membered and three six-membered chelate rings, has a higher

Table 3. Comparison of formation constants (log β_{110}) for selected pentaamine ligands

Polyamine[a]	Co^{II}	Ni^{II}	Zn^{II}	Cd^{II}
ditame	12.8	17.8	11.4	8.7
tetren	13.4	17.4	15.1	13.8
[15]aneN5	16.8[b]		17.9	18.0
[16]aneN5	16.0[b]	17.7	17.9	18.1
pydien	14.8	19.2	13.7	
pydpt	11.5	15.4	11.2	

[a] $\beta_{110} = [ML] \times [M]^{-1} \times [L]^{-1}$; the data are from ref.[53] and are given for 25 °C and an ionic strength of 0.1 M unless otherwise noted; abbreviation of ligands (see also Scheme 1): tetren: 1,4,7,10,13-pentaazatridecane, [15]aneN5: 1,4,7,10,13-pentaazacyclopentadecane, [16]aneN5: 1,4,7,10,13-pentaazacyclohexadecane, pydien: 1,9-bis(2-pyridyl)-2,5,8-triazanonane, pydpt: 1,11-bis(2-pyridyl)-2,6,10-triazaundecane. [b] 35 °C.

Table 2. Formation constants (log β_{xyz}) of ditame complexes (25 °C) with estimated standard deviations in parenthesis (0.1 M KNO_3 or 0.1 M KCl as indicated)

x y z[a]	Co^{II}		Ni^{II}		Zn^{II}		Cd^{II}	
	KNO_3	KCl	KNO_3	KCl	KNO_3	KCl	KNO_3	KCl
1 1 0	12.79(2)	12.93(1)	17.77(2)	17.77(2)	11.43(2)	11.35(1)	8.67(2)	8.19(2)
1 1 1	18.6(2)	18.80(6)	22.42(8)	22.58(8)	19.12(1)	19.03(1)	16.79(2)	16.63(2)
1 1 2	24.8(2)	24.8(2)	27.4(2)	27.7(2)	24.90(6)	25.32(3)	24.02(4)	24.25(2)
1 1 −1	1.04(8)	1.01(6)	5.8(1)	6.6(1)	−0.41(4)	0.96(2)	−2.98(5)	−3.05(3)

[a] $\beta_{xyz} = [M_xL_yH_z] \times [M]^{-x} \times [L]^{-y} \times [H]^{-z}$.

Table 4. Comparison of formation constants (log β_{110}) for some relevant polyamine ligands

Ligand[a]	Denticity	No. of chelate rings five-/six-membered	Co^{II}	Ni^{II}	Zn^{II}	Cd^{II}
ditame[b]	5	0/6	12.8	17.8	11.4	8.7
3,3-tri	3	0/2	6.9	9.2	7.9	6.6
2,2-tri	3	2/0	8.0	10.6	8.8	8.2
tamm[c]	3	0/3	6.3	9.9		5.4
tame[d]	3	0/3		10.1	6.6	
stn[b,e]	6	0/6	10.9	15.6	10.6	9.8
sen	6	3/3	18.0[f]	23.4[b,e]	16.9[b,e,g]	13.4[f]

[a] $\beta_{110} = [ML] \times [M]^{-1} \times [L]^{-1}$; the values given are for $T = 25$ °C, $\mu = 0.1$ M, and are from ref.[53] unless otherwise noted; abbreviation of ligands: 3,3-tri: 1,5,9-triazanonane, 2,2-tri: 1,4,7-triazaheptane, tamm: tris(aminomethyl)methane, tame: 1,1,1-tris(aminomethyl)ethane, stn: 1,1,1-tris(5-amino-2-azapentyl)ethane, sen: 1,1,1-tris(4-amino-2-azabutyl)ethane. For ditame, stn, and sen: see also Scheme 2. [b] This work. [c] 20 °C. [d] 0.5 M KCl. [e] The following pK_a values were used for H_6L^{6+} (25 °C, 0.1 M KCl): 10.92, 10.15, 9.56. 8.52, 6.49, 3.71 for L = stn; and 10.53, 9.61, 9.03, 6.74, 4.70, ca. 2.1 for L = sen. See Tables S4 and S5 in the Supporting Information for further details. [f] 0.5 M KCl.[54] [g] A value $\log\beta_{110} = 17.0(1)$ is reported for 0.5 M KCl.[54]

proportion of such protonation products (Figure S2). The detachment of an amino group in $[Ni(ditame)(H_2O)]^{2+}$ is obviously a particularly unfavorable process, and ditame appears to be unique within the family of ligands forming exclusively six-membered chelate rings.

Formation of Cu^{II} Complexes in Aqueous Solution

Comparison of Ni^{II} and Cu^{II} complex formation with ditame in aqueous solution reveals significant differences. When a 1:1 mixture of $H_5ditame^{5+}$ and Ni^{II} is titrated with 5 equiv. of base, a single, continuous buffer region is observed, according to the reaction $H_5ditame^{5+} + Ni^{2+} + 5\ OH^- \rightarrow [Ni(ditame)]^{2+} + 5\ H_2O$. For Cu^{II}, two individual buffer regions are observed (Figure S3), corresponding to the abstraction of three and of two protons from $H_5ditame^{5+}$ in two sequential and separated steps. It is noteworthy that for the second buffer region, the curve of Cu^{II} lies above that of Ni^{II}, indicating that binding of subsequent amino groups to Ni^{II} is favored at this stage.

For further characterization of the Cu complexes formed, the titration was monitored photometrically. This method allowed the assignment of a spectrum to each individual colored species (Figure S4). The first buffer region could unambiguously be evaluated in terms of $[Cu(H_2L)]^{4+}$ formation (Figure 6). This protonated species predominated in the range $4 < pH < 6$. A meridional coordination mode with two detached $-CH_2-NH_3^+$ branches is proposed for this complex. This assignment is supported by the characteristics of the d-d band with $\lambda_{max} = 619$ nm in comparison to $\lambda_{max} = 616$ nm reported for $[Cu(3,3\text{-tri})]^{2+}$.[55] E. Prenesti et al. reported an empirically derived equation for the estimation of λ_{max} in equatorially coordinated Cu^{II}(amine) complexes,[56] yielding a value of 608 ± 10 nm for such a meridional triamine configuration.

A conclusive assignment for the species appearing in the second buffer region was more difficult. According to the potentiometric measurements, a species of composition Cu^{II}/ditame/H^+ = 1:1:0 was finally formed. The titrations could be interpreted by the assumption of the formation of the simple $[Cu(ditame)]^{2+}$ complex. The corresponding

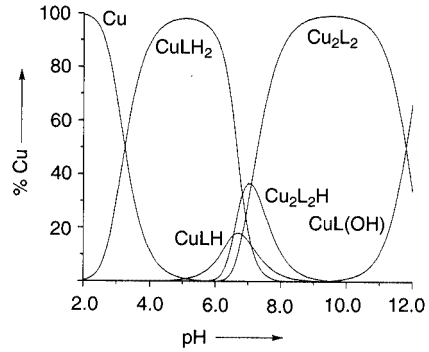

Figure 6. Species distribution plots for equilibrated aqueous solutions with total Cu and total ditame concentration of 10 mM; only metal-containing species are shown; the abundance is given in % of total Cu rather than the amount of species formed; the equilibrium constants listed in Tables 1 and 5 were used for the calculations

λ_{max} of 567 nm, however, is indicative of a tetraammine configuration with the four nitrogen atoms all equatorial.[57] For CuN_5 coordination with an additional nitrogen at the apex, a shift of about 50 nm to *longer* wavelengths would be expected ("pentaamine effect").[4,58] Interestingly, the spectral properties of this species strongly depend on the solvent. Addition of glycerol to a complex solution at pH = 9 resulted in a significant shift of λ_{max} to longer wavelengths (Figure S5). For a glycerol content of 20%, λ_{max} was found at 606 nm. Upon further addition of glycerol this value remained constant. This change can be interpreted as an equilibrium between two different complexes with a Cu^{II}/ditame/H^+ = 1:1:0 composition. An obvious choice for such an equilibrium is the dimerization $2\ [CuL]^{2+} \rightleftarrows [Cu_2L_2]^{4+}$, with the monomer having the square-pyramidal CuN_5 ($\lambda_{max} = 606$ nm) and the dimer a square-planar CuN_4 ($\lambda_{max} = 567$ nm) chromophore. Obviously, $\Delta G°$ for the dimerization is close to 0 under the experimental conditions and this equilibrium is sensitive to subtle changes in the solvent. A conceivable structure for such a dimer would consist of two Cu^{II} centers bonded to the primary amino groups of two ditame ligands. Various conformers of this type, with Cu···Cu separations of 4.0−7.5 Å, were analyzed

by Molecular Mechanics calculations.[59] The structure shown in Figure 7 was found to be of particularly low strain and so can be regarded as a possible model for such a dimer. A series of potentiometric titrations with variable total Cu concentration and variable total Cu/total ditame ratios was now performed, and these measurements could be interpreted well by assuming $[Cu_2L_2]^{4+}$, $[Cu_2L(HL)]^{5+}$, and $[Cu(HL)]^{3+}$ as relevant species (Table 5, Figure 6). The formation of some other Cu^{II} dimers with branched polyamine ligands has recently been described.[60] The spectra of the two dinuclear species $[Cu_2L_2]^{4+}$ and $[Cu_2L(HL)]^{5+}$ did not differ significantly. This is in keeping with the structure shown in Figure 7, in which one of the noncoordinating, secondary nitrogen atoms may be protonated, possibly through intramolecular N−H···N hydrogen bond formation.

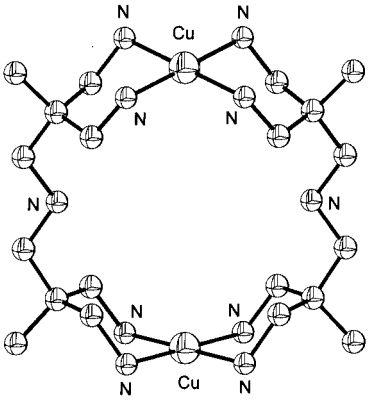

Figure 7. Minimum-energy structure (hydrogen atoms omitted for clarity), calculated by Molecular Mechanics,[59] for the $[Cu_2(ditame)_2]^{4+}$ complex with a square-planar arrangement of the tetraamine donor set; the possible binding of an additional solvent (= H_2O) molecule in the apical positions is omitted in this graphical representation

Table 5. Final model (log $\beta_{x\,y\,z}$) of the Cu(ditame) system (25 °C, 1.0 M KNO_3)

$x\ y\ z$	log $\beta_{x\,y\,z}$[a]
1 1 1	25.5
1 1 2	32.6
1 1 −1	7.1
2 2 0	39.8
2 2 1	46.9

[a] Estimated standard deviations are 0.1 or less.

Further addition of base to an aqueous $[Cu_2L_2]^{4+}$ solution resulted in formation of the hydroxo complex $[CuL(OH)]^+$. This species has a λ_{max} of 606 nm, which is in agreement with an elongated octahedral structure, with N^{sec} and the OH^- ligand in the apices.[58] A pK_a of about 11 was estimated for the $[CuL(OH_2)]^{2+} \rightleftarrows [CuL(OH)]^+ + H^+$ equilibrium. Obviously, $[CuL(OH_2)]^{2+}$ is a slightly stronger acid than the corresponding Co^{II}, Ni^{II}, Zn^{II}, and Cd^{II} complexes.

EPR Characteristics of $[Cu_2(ditame)_2]^{4+}$

For unambiguous identification of the dimer, a comprehensive EPR investigation was performed. The addition of DMSO to a Cu(ditame) complex solution at pH = 9, unlike that of glycerol, did not result in any spectral changes (λ_{max} remained at 567 nm). Most of the low-temperature experiments were therefore performed in frozen DMSO/water solutions. CW EPR measurements were performed primarily to verify the existence of dimers. Figure 8 shows the CW EPR spectra of frozen solutions (2.5 mM Cu) in H_2O with 10% DMSO at pH = 9 (**4**), 10% DMSO at pH = 12 (**5**), and 50% glycerol at pH = 9 (**6**) in the field ranges 260−360 mT (a) and 120−200 mT (b). Simulation parameters for the three samples are given in Table 6. The low-field signal of **4** belongs to the $\Delta M_s = \pm 2$ transitions and arises from magnetic dipole couplings between two Cu^{II} ions. The observation of this low-field spectrum unambiguously shows that sample **4** contains dimers. However, the lack of such a signal in the spectra of **5** and **6** does not necessarily mean that these copper complexes are monomers, since the $\Delta M_s = \pm 2$ transitions can be very low in intensity and difficult to detect. The ratio of the intensity of the forbidden $\Delta M_s = \pm 2$ to the allowed $\Delta M_s = \pm 1$ transitions can be used to estimate the Cu−Cu distance r by the expression[61] $r = [k/I_r(9.1/\nu)^2]^{1/6}$, where k is a constant of approximately 20, I_r is the relative intensity, and ν the microwave frequency. For the dimer of sample **4**, $I_r = 4.4 \cdot 10^{-4}$ yields a distance $r = 5.9$ Å. This estimate is consistent with the proposed structure of the dimer (Figure 7).

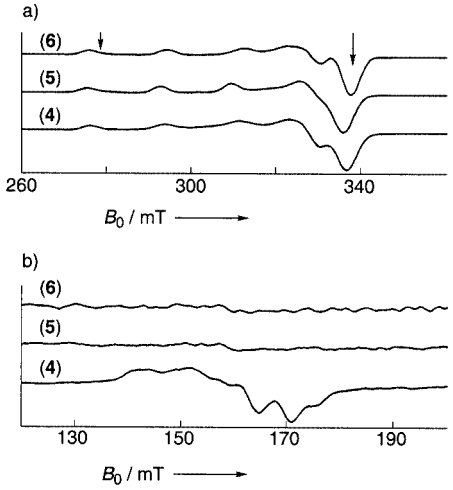

Figure 8. CW EPR spectra of Cu^{II}(ditame); (a) allowed transitions $\Delta M_s = \pm 1$ recorded at 120 K; (b) low-field forbidden transitions $\Delta M_s = \pm 2$ recorded at 10 K; samples: 2.5 mM Cu(ditame) in H_2O with 10% DMSO at pH = 9 (**4**), 10% DMSO at pH = 12 (**5**) and 50% glycerol at pH = 9 (**6**); the two arrows in (a) indicate the observer positions used in ENDOR and HYSCORE experiments

Further information on the coordination of ^{14}N and ^1H nuclei was achieved through ENDOR and HYSCORE experiments.[62] ENDOR spectra on all three samples showed signals from strongly coupled ^{14}N nuclei with hyperfine couplings A between 28 and 34 MHz overlapping with the

Table 6. Principal values of g and A^{Cu} of Cu(ditame) complexes derived from CW EPR

Sample	$g_{\parallel}$	$g_{\perp}$	$\lvert A_{\parallel}^{Cu}\rvert$ [MHz]	$\lvert A_{\perp}^{Cu}\rvert$ [MHz]
^{63}Cu(ditame) in H_2O with				
10% DMSO at pH = 9 (**4**)	2.227	2.051	550	45
10% DMSO at pH = 12 (**5**)	2.238	2.050	530	35
50% Glycerol at pH = 9 (**6**)	2.222	2.048	560	45

signals from weakly coupled ^{1}H nuclei. Spectra from the Cu/ditame dimer sample (Figure 8, sample **4**) taken at the two observer positions indicated in Figure 8a are shown in Figure 9. With weak and long microwave pulses the proton signals dominate, whereas with strong and short microwave pulses the signals of the weakly coupled ^{1}H nuclei are attenuated and the nitrogen signals centered at $A/2$ become clearly visible. The hyperfine couplings of the ^{14}N nuclei are typical for equatorially coordinated nitrogen nuclei with the unpaired electron in the $d_{x^2-y^2}$ orbital of the copper(II) ion.[63]

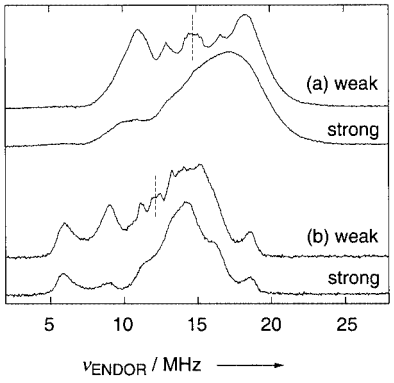

Figure 9. Davies-ENDOR spectra of 2.5 mM Cu(ditame) in H_2O with 10% DMSO at pH = 9 (**4**); spectra were recorded at $g_{\perp}$ (a) and $g_{\parallel}$ (b) by use of weak and strong microwave pulses, respectively (see arrows in Figure 8a); the dashed lines indicate the ^{1}H Larmor frequency

Figure 10 shows two HYSCORE spectra recorded at the high-field position indicated by the arrow in Figure 8a. The spectrum in Figure 10a was measured on the dimer sample **4** and shows large couplings from equatorial ^{1}H nuclei. The spectrum in Figure 10b was measured on sample **5**. In addition to the equatorial ^{1}H nuclei, signals from a ^{14}N nucleus are observed, as indicated in the Figure. Simulations of the ^{14}N HYSCORE spectra, measured at several field positions (Figure S6), resulted in the hyperfine couplings $A_{iso} = -5.6$ MHz, $A_{\parallel} - A_{iso} = 1.8$ MHz, $A_{\perp} - A_{iso} = -0.9$ MHz, and in the nuclear quadrupole coupling $|e^2qQ/h| = 1.3$ MHz with the asymmetry parameter $\eta = 0.4$. They allowed assignment to an axially coordinated ^{14}N nucleus, in agreement with the proposed structure for the monomeric complex. By use of the point-dipole model,[62] the hyperfine anisotropy is given by $T = (\mu_o/2\pi)(gg_n\beta_e\beta_n/hr^3)$. For $T = 0.9$ MHz, a distance of $r = 1.9$ Å between the nitrogen atom and the electron is calculated, a value consistent with expectations. The proton HYSCORE spectra for both complexes show hyperfine couplings of up to 13 MHz, consistent with the ENDOR data.

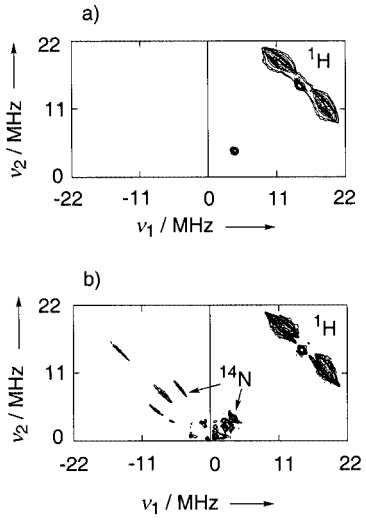

Figure 10. HYSCORE spectra recorded at the high-field position (arrow in Figure 8a) for: 2.5 mM Cu(ditame) in H_2O with 10% DMSO at pH = 9 (Figure 8, sample **4**) (a), 10% DMSO at pH = 12 (Figure 8, sample **5**) (b)

Electrochemistry

Cyclic voltammograms of $[Co(ditame)(H_2O)]^{3+/2+}$ were recorded by use of a hanging Hg drop electrode. Attempts to measure CVs with Au, Pt, or glassy carbon electrodes were not successful. CV scans in neutral and alkaline aqueous solutions showed one single redox step with a strongly pH-dependent potential $E_{obs}^{1/2}$, which decreased with increasing pH in the range $6 < pH < 13$. In aqueous 0.1 M KNO_3, the peak separation ΔE_P was 0.086 V at a scan rate v of 10 mV/s, increasing to $\Delta E_P = 0.162$ V at $v = 200$ mV/s (pH = 9). The ratio of the anodic and cathodic peak current I_{pa}/I_{pc} was 1.0, and I_{pc} depended linearly on $v^{0.5}$. All these observations are in agreement with quasi-reversible electron transfers. The pH dependence was interpreted in terms of a deprotonation of the coordinated water ligand. The species $[Co^{II}L(H_2O)]^{2+}/[Co^{II}L(OH)]^{+}$ ($pK_a^{II} = 11.75$) and $[Co^{III}L(OH_2)]^{3+}/[Co^{III}L(OH)]^{2+}$ ($pK_a^{III} = 6.38$) were taken into consideration. For $pK_a^{III} < pH < pK_a^{II}$, $E_{obs}^{1/2}$ corresponded to an intermediate between the values of the aqua and the hydroxo couples (Figure 11),[24] giving $E^{1/2} = -0.15(1)$ V for $[Co(ditame)(H_2O)]^{3+/2+}$ and $E^{1/2} = -0.47(1)$ V for $[Co(ditame)(OH)]^{2+/+}$ (vs. NHE). For comparison, the corresponding ammine and chloro complexes $[Co(ditame)(NH_3)]^{3+}$ and $[Co(ditame)Cl]^{2+}$ were also studied; they exhibited quasireversible redox behavior with $Co^{3+/2+}$ potentials of -0.41 and -0.20 V (Au electrode), respectively.

CV measurements were performed on the dinuclear Co^{III} complex by use either of the peroxo or of the superoxo forms as starting materials (1 M KCl, Au electrode). Quasireversible redox behavior was found with $E^{1/2} = 0.72$ V vs.

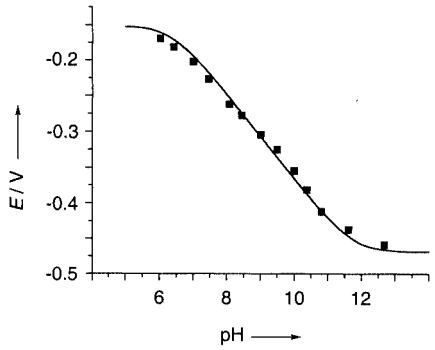

Figure 11. Observed redox potentials $E^{1/2}_{obs}$ for the $[Co(ditame)(OH_2)]^{3+/2+}$ – $[Co(ditame)(OH)]^{2+/+}$ system; squares represent the measured values; the line was calculated by use of the equation $E^{1/2}_{obs} = E^{1/2}{}_{Co^{III/II}L(H_2O)} - RT/F \times \ln\{(1 + K^{III}_a/[H^+])/(1 + K^{II}_a/[H^+])\}$ with $pK^{III}_a = 6.36$, $pK^{II}_a = 11.75$, and $E^{1/2}{}_{Co^{III/II}L(H_2O)} = -0.15$ V; $E^{1/2}{}_{Co^{III/II}L(OH)}$ can be calculated as $E^{1/2}{}_{Co^{III/II}L(H_2O)} - 2.303\ RT/F \times (pK^{II}_a - pK^{III}_a) = -0.47$ V

NHE. This value showed no significant pH dependence in the range $3 < pH < 8$. ΔE_P increased steadily with increasing v ($\Delta E_P = 70$ mV at $v = 10$ mV/s, $\Delta E_P = 120$ mV at $v = 200$ mV/s). I_{pc} was again found to depend linearly on $v^{0.5}$. I_{pa}/I_{pc} varied between 0.8 and 1.2. Similar behavior has been reported for other dinuclear, peroxo-bridged (pentaamine)Co^{III} complexes, with $E^{1/2}_{obs}$ being assigned to reversible oxidation of the O_2^{2-} bridge.[7,15,35,48,64]

In aqueous solutions of $[Ni(ditame)]^{2+}$ (0.1 M KNO_3), cyclic voltammetry indicated formation of an Ni^{III} species. A quasi-reversible one-electron transfer was observed, with $E^{1/2}_{obs} = 0.95$ V vs. NHE ($\Delta E_P = 79$ mV, $v = 5$ mV/s, Au electrode). ΔE_P again increased with increasing v. Unlike in the case of the Co complexes, I_{pa}/I_{pc} depended significantly on v, with $I_{pa}/I_{pc} < 1$ for $v < 100$ mV/s. At $v > 100$ mV/s the ratio was close to unity. $E^{1/2}_{obs}$ did not depend on H^+ concentration in the range $7 < pH < 11$. At higher pH values a significant drop in the potential was noted. Under these conditions, however, the reaction was no longer reversible, and deposition of solid materials on the surface of the electrode was observed. The electrochemical oxidation of Ni^{II}(polyamine) complexes to corresponding Ni^{III} species is well established.[65,66] For $[Ni(sen)]^{3+/2+}$, $E^{1/2}_{obs} = 0.92$ V has been reported.[66] The absence of any pH dependence for the $[Ni(ditame)]^{3+/2+}$ couple at $pH < 11$ is a clear indication that deprotonation of an acidic aqua ligand in the Ni^{III} species does not occur.[67,68] This could be attributable to the Jahn–Teller distortion caused by the low-spin d^7-electron configuration. The drastic drop in the potential at higher pH is coupled with decomposition. A possible explanation of this reactivity would be N–H deprotonation of a coordinated amino group, followed by an intramolecular oxidation of the ligand by Ni^{III}.[68,69]

Conclusions

The pentadentate ditame ligand (= L) forms $[NiLX]^{2+}$ complexes (X = solvent molecule) of surprisingly high stability and selectivity. We attribute the high selectivity to the peculiar ligand geometry, which appears to be particularly well suited for accommodation of late transition metal ions of fairly small size and a distinct preference for octahedral coordination. This conclusion is based on the following observations:

(i) ditame and stn (Scheme 1) can both be regarded as extensions of the tripodal tris(aminomethyl)ethane (tame), with exclusive formation of six-membered chelate rings. However, with respect to $[NiL]^{2+}$ formation, the complex with the *penta*dentate ditame is significantly more stable than the complex with the *hexa*dentate stn. The situation is different for Cd^{II}, for which the complex with stn is of slightly higher stability.

(ii) The favorable geometry of ditame for Ni^{II} binding is further demonstrated by the low capacity of $[Ni(ditame)]^{2+}$ to dissociate partially and to protonate an amino group. This type of reactivity is usually a feature of polyamine complexes with multiple six-membered chelate rings. For $[Zn(ditame)]^{2+}$, partial dissociation and partial protonation of the ligand is indeed extensively observed.

(iii) The geometry of ditame appears to induce a rather short $M-N^{sec}$ bond. This feature is most readily attained in complexes with an approximately octahedral structure. As a consequence, $[Cu(ditame)]^{2+}$ has a rather low stability, which does not fit normal Irving–Williams behavior. Two primary amino groups are readily detached and protonated, forming a meridional $[Cu(H_2ditame)]^{4+}$ complex, which appears to predominate in slightly acidic solutions. Furthermore, the EPR measurements provided unambiguous evidence that in slightly alkaline solution, in which the noncoordinating ammonium groups of $[Cu(H_2ditame)]^{4+}$ become deprotonated, the mononuclear species is in equilibrium with a dimer, $[Cu_2(ditame)_2]^{4+}$. In this dimer, Cu^{II} is probably bonded to the four primary amino groups with a square-planar arrangement.

From the high stability and the possibility for additional binding of a monodentate entity X (a "substrate"), octahedral complexes such as $[NiLX]^{2+}$ or $[CoLX]^{3+}$ would have ideal prerequisites for synthetic or even catalytic applications. The dimeric Co^{III}(peroxo)/(superoxo) complexes $\mathbf{2}^{4+}$ and $\mathbf{3}^{5+}$, in which reversible one-electron transfer was observed for the dioxygen bridge over a wide pH range (2–9), may be regarded as models for this type of reactivity.

Experimental Section

Materials and Instrumentation: ditame·5HCl,[21] [Co(ditame)Cl][$ZnCl_4$],[21] [Co(ditame)(NH_3)]Cl[$ZnCl_4$],[21] sen·6HCl,[26] and stn·6HCl[26] were prepared as described. Unless otherwise stated, all chemicals used for the synthetic work were commercially available products of reagent-grade quality. H_2O was distilled twice (quartz apparatus). Organic solvents were purified by distillation prior to use. For the potentiometric and spectrophotometric titrations, metal salts of the highest available quality (> 99.95%) were used. $^{63}CuCl_2$ (for EPR) was purchased (98.6% isotopically enriched) from CAMPRO Scientific (Berlin, Germany). Dowex 50 W-X2 (100–200 mesh, H^+ form) and Dowex 2-X8 (50–100 mesh,

Cl^- form) were purchased from Fluka. The anion resin was converted into the OH^- form or the NO_3^- form by use of 0.3 M aqueous NaOH or concd. KNO_3, respectively. UV/Vis spectra of the Ni^{II} complexes were measured with a Uvikon 941 spectrophotometer (H_2O, 25±3 °C), while a solid-state UV/Vis spectrum of **2**Cl_4·$4H_2O$ was recorded with sapphire plates and a Cary 5 spectrometer. IR spectra were recorded with a Bruker Vector 22 FT IR spectrometer equipped with a Golden Gate ATR unit. Raman spectra were measured with a Dilor-XY spectrometer, with an Ar^+/Kr^+-mixed gas laser used for excitation (λ = 647.1 nm). C,H,N analyses were performed by H. Feuerhake (Universität des Saarlandes).

Measurement and Interpretation of NMR Spectra: ^1H and $^{13}C\{^1H\}$ NMR spectra were measured in D_2O (28 °C) with a Bruker DRX 500 spectrometer (resonance frequencies: 500.13 MHz for ^1H and 125.9 MHz for ^{13}C). Chemical shifts (in ppm) are given relative to sodium [D_4](trimethylsilyl)propionate as an internal standard (δ = 0 ppm). A Hamilton SPINTRODE glass electrode, fitted with an internal Ag/AgCl reference (H_2O), was used within the NMR tube for a direct measurement of pD (corrected).[29] Least-squares calculations [$\Sigma(\delta_{obs} - \delta_{calc})^2$ = min] were performed with the computer program NMR-Tit,[70] the resulting parameters (pK_a and δ_{calc}) of the macro species are listed in Table S1. The constants P^α, S^α, P^χ, and S^χ were used to model the deshielding of the CH_2 and CH_3 protons in the individual microspecies caused by protonation of a primary (*P*) or the secondary (*S*) amine site, respectively. The distances between the protonated site and the hydrogen atom under consideration are indicated as α (N−C−H) and χ (N−C−C−C−H). Effects over longer distances were not considered. From symmetry arguments, the protonation of a primary amino group was always treated in a statistical manner by distributing the protons equally over all four sites. Because of the low number of observations (i.e., the resonances X, Y, Z in Figure 1), the same distance dependence was assumed for the primary and the secondary amine sites: $P^\chi/P^\alpha = S^\chi/S^\alpha = x$. From the data for the fully protonated and the fully deprotonated form one obtains: (i) $P^\alpha + xP^\alpha + xS^\alpha = 0.89$; (ii) $S^\alpha + 2x\,P^\alpha = 1.066$; (iii) $2xP^\alpha + x\,S^\alpha = 0.558$; and subsequently $P^\alpha = 0.495$, $S^\alpha = 0.748$, and $x = 0.32$. It is noteworthy that the value of 0.32 for *x* is significantly larger than corresponding ratios previously reported for methylene groups of macrocyclic polyamines.[31] The observed shifts of the macrospecies HL^+, H_2L^{2+}, H_3L^{3+}, and H_4L^{4+} were then interpreted as weighted averages of the two micro species (Table S2).

EPR: CW EPR measurements were performed with a Bruker ESP300 spectrometer (microwave frequency 9.43 GHz) equipped with a liquid nitrogen cryostat and a liquid helium cryostat from Oxford Inc. HYSCORE and ENDOR experiments[62] were carried out at X-band frequencies with a Bruker Elexsys spectrometer (microwave frequency 9.68 GHz) at 20 K. The HYSCORE experiments with the pulse sequence $\pi/2-\tau-\pi/2-t_1-\pi-t_2-\pi/2-\tau-$echo used 40-ns $\pi/2$ pulses, a 16-ns transfer π pulse, and an eight-step phase cycle. Two Davies-ENDOR experiments were measured by using the pulse sequence $\pi-T-\pi/2-\tau-\pi-$echo. One sequence employed a 120-ns π pulse and the second sequence employed a 32-ns π pulse to suppress weakly coupled proton nuclei. A radio frequency pulse with a length of 8 μs and a flip angle of π for the matrix protons was used. All measurements were carried out in frozen aqueous solutions with addition of DMSO or glycerol, using ^{63}Cu. Oxygen-free samples were obtained by degassing (freeze-pump-thaw method under vacuum). CW EPR and HYSCORE simulations were calculated with the EasySpin package[71] and the TRYSCORE program,[72] respectively.

Electrochemistry: Cyclic voltammograms of $[CoL(NH_3)]^{3+/2+}$, $[CoLCl]^{2+/+}$, $[NiL(H_2O)]^{3+/2+}$, and $[Co_2L_2(O_2)]^{5+/4+}$ (L = ditame) were recorded with a BAS C2 cell and a BAS 100B/W 2 potentiostat at ambient temperature (23±3 °C) with an Au working electrode, a Pt counter-electrode, and an Ag/AgCl reference. The $[CoL(H_2O)]^{3+/2+}$ couple was investigated by using an Hg (hanging drop) working electrode and $Na_2B_4O_7$·$10H_2O$ or 4-(2-hydroxyethyl)piperazin-1-propanesulfonic acid (HEPPS) as buffers. Potentials quoted were calculated relative to the normal hydrogen electrode (NHE), with a value of 0.46 V used for the $[Fe(CN)_6]^{3-/4-}$ couple (0.01 M NaOH).

Potentiometric Measurements: Potentiometric titrations (50 mL sample solution) were carried out under nitrogen at 25.0±0.1 °C as described previously.[4,29] Solid, analytically pure samples of ditame·5HCl, ditame·$5HNO_3$·$0.5H_2O$, stn·6HCl·$2H_2O$, or sen·6HCl were applied to determine the pK_a values of the ligands. Metal-containing samples (Co, Ni, Cu, Zn, Cd) were prepared from standardized aqueous stock solutions (w/w) of the metal chlorides or metal nitrates. Details of the various titrations are summarized in Tables S3−S5. Formation of Ni^{II} complexes with sen and stn proved to be too slow for continuous titration, and a batch method with individually sealed sample solutions was applied.

Spectrophotometric Titrations: The titration cell used for the potentiometric titrations was equipped with an immersion probe (HELLMA) connected to a diode array spectrophotometer (J&M, TIDAS-UV/NIR/100-1). An in-house computer program was used to control the addition of the titrant (1 M KOH) and to trigger a spectrum of the sample solution (0.01−0.02 M total Cu, 1 M KNO_3, 25.0±0.1 °C) prior to the addition of each aliquot of titrant.

Calculations of Equilibrium Constants: All equilibrium constants were calculated as concentration constants and the pH was defined as $-\log [H^+]$. The potentiometric data were evaluated by use of the computer program HYPERQUAD.[73] The pK_w (13.78 for μ = 0.1 M, 13.71 for μ = 1.0 M)[53] and the total concentrations of the reactants were treated as fixed values. Additionally, the protonation constants of the ligands were also fixed (Table 1) when refining formation constants of metal-containing species. The model for Cu(ditame) complexes was established by collective evaluation of several titration experiments with total Cu and total ditame concentrations ranging from 0.25 to 10.0 mM. The spectrophotometric data were evaluated by use of the computer program SPECFIT.[74] The spectrum of the free Cu^{2+} was measured separately and was not refined; ditame and its protonation products were regarded as colorless.

Crystal Structure Determination:[75] X-ray diffraction data of **1**Br_2, **2**Cl_4·$4H_2O$, and **3**$Cl_2[ZnCl_4][ZnCl_3(H_2O)]$·$H_2O$ were collected with a STOE imaging Plate Diffraction System by use of graphite-monochromatized Mo-K_α radiation (λ = 0.71073 Å) at 25(2) °C. Further details are summarized in Table 7. No indication of crystal decay was noted for any of the crystals during data collection. All data sets were corrected for Lorentz and polarization effects. *Specific comments for* ***1****Br*$_2$ *and* ***2****Cl*$_4$·$4H_2O$*:* The symmetries of diffraction patterns and systematic extinctions were consistent with space group types *Pnma* and $Pna2_1$ for **1**Br_2, and *I*2/*m*, *Im*, and *I*2 for **2**Cl_4·$4H_2O$. The structures were solved by direct methods.[76] Approximate positions of all the hydrogen atoms were found in different stages of refinements by full-matrix, least-squares calculations on F^2.[77] Refinements suffered from the high pseudosymmetry of the cations $\mathbf{1}^{2+}$ and $\mathbf{2}^{4+}$ and the possibility of disorder on sites of higher symmetry had to be taken into account with respect to their

shape and the symmetry of their solid-state environments. In both cases, none of the possible space groups allowed a complete set of physically reasonable atomic and anisotropic displacement parameters to be refined without use of appropriate weak restraints to overcome correlation problems. Consistent with E-statistics, significantly better results were observed for a model with 1:1 orientationally disordered cations on a site of symmetry *m* in centrosymmetric space group *Pnma* in the case of $\mathbf{1}Br_2$ ($S = 1.06$), and for a C_2-symmetric model on a site of corresponding symmetry in the chiral space group *I*2 in the case of $\mathbf{2}Cl_4{\cdot}4H_2O$ ($S = 1.07$).[77] The absolute structure of $\mathbf{2}Cl_4{\cdot}4H_2O$ could be determined reliably.[78] Anisotropic displacement parameters were refined for all non-hydrogen atoms with the exception of O4 and O5, representing disordered water molecules of $\mathbf{2}Cl_4{\cdot}4H_2O$ in partially occupied general positions (occupation 0.25 and 0.25). All H atoms were treated with fixed idealized O−H, N−H, or C−H distances. With idealized geometries assumed for the CH_3, CH_2, NH_2, and NH groups, the riding model was applied for the H atoms. In addition, the H atoms of methyl groups were allowed to move collectively around the neighboring C−C axis. The water molecules of $\mathbf{2}Cl_4{\cdot}4H_2O$ were treated as rigid groups with idealized bond lengths and angles. The orientation of the OH group of the ethanol ligand of $\mathbf{1}^{2+}$ was refined. Isotropic displacement parameters of H atoms were kept equal to 120% of the equivalent isotropic displacement parameters of the parent oxygen, nitrogen, and carbon atoms for the OH, NH, NH_2, and CH_2 groups and equal to 150% for the CH_3 groups and water molecules. *Specific comments for* $\mathbf{3}Cl_2[ZnCl_4]{\cdot}[ZnCl_3(H_2O)]{\cdot}H_2O$: The structure was solved by direct methods (SHELXS-97) and refined by full-matrix, least-squares calculations on F^2 by use of SHELXL-97.[76,77] One water molecule of crystallization (O2) was found to be distributed over three sites (O2A, O2B, O2B′, with O2B−O2B′ being related by $= -x, y, -z + 1/2$) with site occupancies of 0.28, 0.36, and 0.36. The O(4A)−Cl(4A) part of the two counter-ions $[ZnCl_4]^{2-}$and $[ZnCl_3(H_2O)]^-$ (which were related through a center of inversion), was also found to be disordered. Some preliminary isotropic refinement found an occupancy of 50±2% for O(4A) and Cl(4A). In the final refinement, the occupancy of these atoms was fixed at 50%, and anisotropic displacement parameters were used for all non-hydrogen atoms. The positions of the H atoms were calculated (riding model with $U_{iso} = 1.2 \times U_{eq}$ of the pivot atom).

Molecular Modeling Calculations: These were carried out with the commercially available program MOMEC97.[59]

[Ni(ditame)(EtOH)]Br_2: ditame·5HCl[21] (2.20 g, 5.50 mmol) was dissolved in H_2O (100 mL) and deprotonated with Dowex 2 (OH^- form). The solution was concentrated to dryness under reduced pressure. The oily residue was redissolved in H_2O (20 mL), and a solution of $NiBr_2{\cdot}3H_2O$ (1.47 g, 5.39 mmol) in H_2O (20 mL) was added dropwise. A color change to violet was noted. The solution was concentrated to dryness, and the residue was recrystallized from EtOH (40 mL)/H_2O (6 mL) at 5 °C. The resulting violet precipitate was washed with EtOH and Et_2O and dried in vacuo over P_2O_5 (1.07 g, 41%). $C_{12}H_{33}Br_2N_5NiO$ (482.0): calcd. C 29.91, H 6.90, N 14.53; found C 30.06, H 6.93, N 14.70. UV/Vis: λ_{max} (ε) = 338 (10.1), 533 (7.6), 884 (9.9) nm. Single crystals suitable for X-ray crystallography were grown by layering a concentrated aqueous complex solution with EtOH.

ditame·5HCl: A high-purity sample required for the potentiometric titrations was obtained from the Ni complex. [Ni(ditame)(EtOH)]Br_2 was recrystallized twice from EtOH/H_2O. The resulting, analytically pure, violet compound was dissolved in H_2O and heated to 50 °C. Concd. HCl was added to the solution in small portions until a color change to green was noted. The clear green solution was diluted with water to pH = 1 and sorbed on Dowex 50. The column was eluted with water and with 0.5 M HCl until all the Ni had been removed (checked with dimethylglyoxime). Elution with 6 M HCl yielded a colorless solution of ditame·5HCl, which was concentrated to dryness. The resulting white solid was recrystallized from concd. HCl/MeOH/EtOH (yield 72%). $C_{10}H_{32}Cl_5N_5$ (399.7): calcd. C 30.05, H 8.07, N 17.52; found C 30.06, H 8.19, N 17.30. ^{1}H NMR (D_2O, pD < 2): δ = 1.27 (s, 6 H), 3.06 (s, 4 H), 3.23 (AB system, 8 H) ppm. ^{13}C NMR (D_2O, pD < 2): δ = 20.1, 38.7, 46.4, 57.0 ppm.

ditame·5HNO$_3$·0.5H$_2$O: ditame·5HCl (1.40 g, 3.50 mmol) was dissolved in H_2O (1400 mL) and sorbed on Dowex 2 (NO_3^- form). The column was eluted *slowly* (over 24 h) with water and the resulting solution was concentrated to dryness. The oily residue was carefully dried in vacuo over P_2O_5, and recrystallized from MeOH/H_2O (yield 72%). $C_{10}H_{33}N_{10}O_{15.5}$ (541.4): calcd. C 22.18, H 6.14, N 25.87; found C 22.32, H 6.14, N 25.59. ^{1}H NMR (D_2O, pD < 2) identical with that of ditame·5HCl.

[Zn(ditame)(EtOH)]Br$_2$: The Zn complex was prepared by the same procedure as reported for the Ni complex and was obtained as a colorless, crystalline solid (38%). $C_{12}H_{33}Br_2N_5OZn$ (488.6): calcd. C 29.50, H 6.81, N 14.33; found C 29.31, H 6.73, N 14.52.

[Co$_2$O$_2$(ditame)$_2$]Cl$_4$·4H$_2$O: ditame·5HCl (800 mg, 2 mmol) was dissolved in H_2O (5 mL) and deprotonated on Dowex 2 (OH^- form). The alkaline eluent was concentrated to dryness under reduced pressure, and the oily residue was redissolved in H_2O (10 mL). $CoCl_2{\cdot}6H_2O$ (476 mg, 2 mmol), dissolved in H_2O (10 mL), was then added dropwise, and a stream of O_2 was passed through the solution over a period of 3 h. The color changed from yellow to deep brown. The solution was allowed to stand for 3 d at 5 °C, and the resulting brown solid was collected by filtration. The remaining clear, brown solution was concentrated to a volume of 20 mL, cooled, and allowed to stand for 3 d at 5 °C. After collection of a second fraction of the product, the two fractions were combined, washed with Et_2O, and dried in vacuo (367 mg, 47%). $C_{20}H_{62}Cl_4Co_2N_{10}O_6$ (798.5): calcd. C 30.09, H 7.83, N 17.54; found C 30.04, H 7.89, N 17.74. UV/Vis: λ_{max} (log ε) = 296 (4.1) nm. IR: $\tilde{\nu}$ = 3358, 3177, 3079, 2954, 2907, 2873, 1603, 1461, 1409, 1202, 1155, 1117, 1083, 1020, 969, 910, 735, 629, 562, 505 cm^{-1}. ^{1}H NMR (D_2O): δ = 0.86 (s, 12 H), 2.36 (4 H), 2.47 (8 H), 2.56 (8 H), 2.73 (4 H) ppm. ^{13}C NMR (D_2O): δ = 23.5, 42.3, 47.8, 49.2, 59.2 ppm. Single crystals suitable for X-ray crystallography were grown from a saturated aqueous solution by slow concentration at room temperature.

[Co$_2$O$_2$(ditame)$_2$]Cl$_5$·2H$_2$O: $[Co_2O_2(ditame)_2]Cl_4{\cdot}4H_2O$ (270 mg, 0.338 mmol) was suspended in H_2O (50 mL). $Ce(SO_4)_2{\cdot}4H_2O$ (140 mg, 0.346 mmol) was separately dissolved in H_2O (10 mL). Both solutions were acidified to pH = 1 with a few drops of 8 M HCl. The Ce^{IV} solution was added rapidly (within 1 min) to the suspension of the μ-peroxo complex, and the resulting deep green solution was stirred for 10 min. EtOH (200 mL) was added, and the mixture was allowed to stand for 72 h at 5 °C. The green precipitate was collected, washed carefully with EtOH and Et_2O, and air-dried (200 mg, 74%). $C_{20}H_{58}Cl_5Co_2N_{10}O_4$ (797.9): calcd. C 30.11, H 7.33, N 17.55; found C 30.25, H 7.30, N 17.16. UV/Vis: λ_{max} (log ε) = 312 (3.9), 471 (2.3), 695 (2.85) nm. Single crystals of composition $\mathbf{5}Cl_2[ZnCl_4][ZnCl_3(H_2O)]{\cdot}H_2O$ suitable for X-ray crystallography were grown at 5 °C from a saturated aqueous solution (10 mL) of the pentachloride salt after addition of a solution (10 mL) of HCl (8 M) and $ZnCl_2$ (1 g).

Table 7. Crystallographic data of $[Ni(ditame)(EtOH)]Br_2$ (**1**Br_2), $[Co_2(ditame)_2O_2]Cl_4{\cdot}4H_2O$ (**2**$Cl_4{\cdot}4H_2O$), and $[Co_2(ditame)_2O_2]Cl_2[ZnCl_4][ZnCl_3(H_2O)]{\cdot}H_2O$ (**3**$Cl_2[ZnCl_4][ZnCl_3(H_2O)]{\cdot}H_2O$)

Complex	$\mathbf{1}^{2+}$	$\mathbf{2}^{4+}$	$\mathbf{3}^{5+}$
Empirical formula	$C_{12}H_{33}Br_2N_5NiO$	$C_{20}H_{62}Cl_4Co_2N_{10}O_6$	$C_{20}H_{58}Cl_9Co_2N_{10}O_4Zn_2$
Formula mass	481.96	798.46	1070.41
Crystal system	orthorhombic	monoclinic	monoclinic
Space group	*Pnma* (no. 62)	*I*2 (no. 5)	*C*2/*c* (no. 15)
a [Å]	20.509(4)	14.291(3)	23.190(5)
b [Å]	7.7354(15)	7.2447(14)	14.244(3)
c [Å]	12.436(3)	18.488(4)	16.165(3)
β [°]	90	108.80(3)	127.97(3)
V [Å^3]	1972.9(7)	1812.0(6)	4209(2)
Z	4	2	4
$D_{calcd.}$ [g cm^{-3}]	1.623	1.463	1.689
μ [mm^{-1}]	5.040	1.257	2.512
Crystal size [mm]	0.4 × 0.1 × 0.1	0.50 × 0.32 × 0.28	0.3 × 0.2 × 0.1
θ_{min}, θ_{max} [°]	1.92, 24.12	3.01, 25.79	1.81, 22.50
Data set	−23/23; −8/8; −14/13	−17/17; −8/8; −22/22	−24/19; 0/15; 0/17
Total/unique data	12136, 1670	12816, 3240	2753, 2753
Parameter/restraints	194/38	198/9	231/0
R_1, wR_2 [$I > 2\sigma(I)$]	0.0462, 0.1075	0.0639, 0.1286	0.0567, 0.1342
R_1, wR_2 (all data)	0.0579, 0.1122	0.0712, 0.1322	0.0579, 0.1348
Abs. struct. param.		0.06(3)	
Max. peak/hole [e/Å^3]	0.907/−0.884	0.541/−0.312	0.593/−0.565

[Co(ditame)(H_2O)](CF_3SO_3)$_3$: [Co(ditame)Cl][$ZnCl_4$][21] (100 mg, 193 μmol) was dissolved in H_2O (10 mL) and sorbed on Dowex 50. The column was washed with H_2O, 0.1 M HCl, 0.5 M HCl, and 1 M HCl (200 mL each). Further elution with 3 M HCl gave a dark red fraction, which was concentrated to dryness. The resulting solid was redissolved in H_2O (20 mL) and heated to 80 °C. A solution of $AgCF_3SO_3$ was added dropwise until the precipitation of solid AgCl was completed. The solid was removed by filtration (Celite) and the reddish-orange, clear solution was concentrated to dryness. (142 mg, 100%). $C_{13}H_{29}CoF_9N_5O_{10}S_3$ (741.5): calcd. C 21.06, H 3.94, N 9.44; found C 21.42, H 4.09, N 9.42. UV/Vis: λ_{max} = 345, 487 nm. ^{1}H NMR (D_2O): δ = 0.93 (s, 6 H), 2.06 (2 H), 2.33 (2 H), 2.45 (2 H), 2.62 (2 H) 2.74 (2 H), 2.77 (2 H) ppm. ^{13}C NMR (D_2O): δ = 22.8, 42.8, 47.1, 48.4, 57.7, 122.3 (q, *J* = 316 Hz) ppm.

[Ni(stn)]$Br_2{\cdot}2.5H_2O$: The procedure reported above for the ditame complex was applied, with $NiBr_2{\cdot}3H_2O$ (534 mg, 1.96 mmol) and crude[26] stn·6HCl·$2H_2O$ (1.09 g, 2 mmol). The resulting violet solid was recrystallized from H_2O (10 mL) and EtOH (20 mL) at 5 °C (70%). $C_{14}H_{41}Br_2N_6NiO_{2.5}$ (552.0): calcd. C 30.46, H 7.49, N 15.22; found C 30.52, H 7.48, N 15.19. UV/Vis: λ_{max} (ε) = 341 (13.9), 539 (10.6), 858 (8.3) nm.

stn·6HCl·$2H_2O$: A high-purity sample required for the titration experiments was prepared from crystalline, analytically pure [Ni(stn)]$Br_2{\cdot}2.5H_2O$ (570 mg, 1.03 mmol). The complex was decomposed by HCl and sorbed on Dowex 50 as described above for ditame·5HCl. The protonated polyamine was eluted with 8 M HCl, and the solution was concentrated to a total volume of 10 mL. MeOH (20 mL) was added slowly, and the mixture was allowed to stand at 5 °C for 72 h. The colorless, crystalline solid was removed by filtration, washed with EtOH and EtOEt, and dried in vacuo (81%). $C_{14}H_{46}Cl_6N_6O_2$ (543.3): calcd. C 30.95, H 8.53, N 15.47; found C 30.90, H 8.57, N 15.28. ^{1}H NMR (D_2O, pD < 3): δ = 1.39 (s, 3 H), 2.18 (m, 6 H), 3.12 (t, *J* = 8 Hz, 6 H), 3.26 (t, *J* = 8 Hz, 6 H), 3.38 (s, 6 H) ppm. ^{13}C NMR (D_2O, pD < 3): δ = 21.0, 26.7, 38.8, 39.6, 49.4, 55.4 ppm.

[Ni(sen)]Br_2:[66] The procedure reported above for the ditame complex was applied, with $NiBr_2{\cdot}3H_2O$ (545 mg, 2 mmol) and crude[26] sen·6HCl (930 mg, 2 mmol). The resulting violet solution was concentrated to a total volume of 10 mL. EtOH (50 mL) was added, and the solution was allowed to stand at 5 °C for 72 h. Violet needles (572 mg, 62%). $C_{11}H_{30}Br_2N_6Ni$ (464.9): calcd. C 28.42, H 6.50, N 18.08; found C 28.72, H 6.56, N 17.77. UV/Vis: λ_{max} (ε) = 337 (10.0), 522 (8.2), 803 (10.0) nm.

sen·6HCl: A high-purity sample required for the titration experiments was prepared from crystalline, analytically pure [Ni(sen)]Br_2 (1664 mg, 3.58 mmol). The complex was decomposed with HCl and sorbed on Dowex 50 as described above for ditame·5HCl. The protonated polyamine was eluted with 8 M HCl and the solution was concentrated to a total volume of 20 mL. MeOH (100 mL) and EtOH (50 mL) were added slowly, and the mixture was allowed to stand at 5 °C for 72 h. The colorless, crystalline solid was removed by filtration, washed with EtOH and EtOEt, and dried in vacuo (1.20 g, 72%). $C_{11}H_{36}Cl_6N_6$ (465.2): calcd. C 28.40, H 7.8, N 18.07; found C 28.30, H 7.86, N 17.69. ^{1}H NMR (D_2O, pD < 3): δ = 1.44 (s, 3 H), 3.47 (s, 6 H), 3.53 (m, 12 H) ppm. ^{13}C NMR (D_2O, pD < 3): δ = 21.1, 38.4, 39.3, 48.9, 55.1 ppm.

Supporting Information: Supporting information for this article is available (see footnote on the first page of this article). Tables S1−S5 list NMR parameters and potentiometric data. Figures S1−S6 show the disorder of [Ni(ditame)(EtOH)]Br_2, pH-dependent species distribution plots of the Co^{II}/ditame, Cd^{II}/ditame, and Ni^{II}/sen systems, titration curves of Cu^{2+}/Ni^{2+}/ditame·$5HNO_3$ solutions, and Vis and EPR data for the Cu(ditame) complexes.

Acknowledgments

The Raman and solid-state UV/Vis spectra were measured by Prof. Dr. Felix Tuczek (Kiel). MM calculations were carried out by Dr. Dirk Kuppert (Saarbrücken). Part of the synthetic work was performed by Anton Zaschka (Saarbrücken). X-ray diffraction data

for $\mathbf{5}Cl_2[ZnCl_4][ZnCl_3(H_2O)]\cdot H_2O$ were recorded by Dr. Volker Huch (Saarbrücken). We thank Stefan Steinhauser and Bernd Morgenstern (Saarbrücken) for valuable help and suggestions. Financial support from the Saarland (O. M.) and the Fonds der Chemischen Industrie (K. H.) is gratefully acknowledged.

[1] [1a] D. S. C. Black, A. J. Hartshorn, *Coord. Chem. Rev.* **1973**, *9*, 219−274. [1b] K. Hegetschweiler, *Chem. Soc. Rev.* **1999**, *28*, 239−249.
[2] [2a] P. Braunstein, F. Naud, *Angew. Chem. Int. Ed.* **2001**, *40*, 680−699. [2b] C. Gambs, S. Chaloupka, G. Consiglio, A. Togni, *Angew. Chem. Int. Ed.* **2000**, *39*, 2486−2488.
[3] T. Bark, M. Düggeli, H. Stoeckli-Evans, A. von Zelewsky, *Angew. Chem. Int. Ed.* **2001**, *40*, 2848−2851.
[4] A. Zimmer, D. Kuppert, T. Weyhermüller, I. Müller, K. Hegetschweiler, *Chem. Eur. J.* **2001**, *7*, 917− 931.
[5] [5a] R. J. Geue, J. V. Hanna, A. Höhn, C. J. Qin, S. F. Ralph, A. M. Sargeson, A. C. Willis, *Adv. Chem. Ser.* **1997**, *253*, 137−150. [5b] A. M. Allgeier, C. A. Mirkin, *Angew. Chem. Int. Ed.* **1998**, *37*, 894−908.
[6] B. M. Gatehouse, G. McLachlan, L. L. Martin, R. L. Martin, L. Spiccia, *Aust. J. Chem.* **1991**, *44*, 351−359.
[7] P. V. Bernhardt, G. A. Lawrance, T. W. Hambley, *J. Chem. Soc., Dalton Trans.* **1990**, 235−241.
[8] J. H. Timmons, A. Clearfield, A. E. Martell, R. H. Niswander, *Inorg. Chem.* **1979**, *18*, 1042−1047.
[9] J. H. Timmons, R. H. Niswander, A. Clearfield, A. E. Martell, *Inorg. Chem.* **1979**, *18*, 2977−2982.
[10] A. Grohmann, F. Knoch, *Inorg. Chem.* **1996**, *35*, 7932−7934.
[11] C. Dietz, F. W. Heinemann, J. Kuhnigk, C. Krüger, M. Gerdan, A. X. Trautwein, A. Grohmann, *Eur. J. Inorg. Chem.* **1998**, 1041−1049.
[12] A. Grohmann, F. W. Heinemann, P. Kofod, *Inorg. Chim. Acta* **1999**, *286*, 98−102.
[13] T. Poth, H. Paulus, H. Elias, R. van Eldik, A. Grohmann, *Eur. J. Inorg. Chem.* **1999**, 643−650.
[14] C. Dietz, F. W. Heinemann, A. Grohmann, *Eur. J. Inorg. Chem.* **1999**, 2147−2156.
[15] S. Schmidt, F. W. Heinemann, A. Grohmann, *Eur. J. Inorg. Chem.* **2000**, 1657−1667.
[16] C. Zimmermann, F. W. Heinemann, A. Grohmann, *Eur. J. Inorg. Chem.* **2001**, 547−555.
[17] D. A. House, *Coord. Chem. Rev.* **1977**, *23*, 223−322.
[18] D. A. House, *Compr. Coord. Chem.* **1987**, *2*, 23−72.
[19] A. Bianchi, M. Micheloni, P. Paoletti, *Coord. Chem. Rev.* **1991**, *110*, 17−113.
[20] [20a] E. Kimura, M. Haruta, T. Koike, M. Shionoya, K. Takenouchi, Y. Iitaka, *Inorg. Chem.* **1993**, *32*, 2779−2784. [20b] T. W. Hambley, G. A. Lawrance, M. Maeder, E. N. Wilkes, *Inorg. Chim. Acta* **1996**, *246*, 65−71. [20c] L. R. Gahan, G. A. Lawrance, A. M. Sargeson, *Aust. J. Chem.* **1982**, *35*, 1119−1131.
[21] B. Fabius, R. J. Geue, R. G. Hazell, W. G. Jackson, F. K. Larsen, C. J. Qin, A. M. Sargeson, *J. Chem. Soc., Dalton Trans.* **1999**, 3961−3972.
[22] D. A. Buckingham, W. G. Jackson, P. A. Marzilli, A. M. Sargeson, *Aust. J. Chem.* **1999**, *52*, 185−204.
[23] M. Zehnder, U. Thewalt, *Z. Anorg. Allg. Chem.* **1980**, *461*, 53−60.
[24] M. Maeder, H. R. Mäcke, *Inorg. Chem.* **1994**, *33*, 3135−3140.
[25] [25a] A. Zimmer, I. Müller, G. J. Reiß, A. Caneschi, D. Gatteschi, K. Hegetschweiler, *Eur. J. Inorg. Chem.* **1998**, 2079−2086. [25b] G. J. Reiss, A. Zimmer, K. Hegetschweiler, *Acta Crystallogr., Sect. C* **2000**, *56*, 284−288.
[26] R. J. Geue, G. H. Searle, *Aust. J. Chem.* **1983**, *36*, 927−935.
[27] [27a] F. J. Millero, D. R. Schreiber, *Am. J. Science* **1982**, *282*, 1508−1540. [27b] F. J. Millero, *Geochim. Cosmochim. Acta* **1992**, *56*, 3123−3132.
[28] J. W. Pauly, J. Sander, D. Kuppert, M. Winter, G. J. Reiss, F. Zürcher, R. Hoffmann, T. F. Fässler, K. Hegetschweiler, *Chem. Eur. J.* **2000**, *6*, 2830−2846.
[29] D. Kuppert, J. Sander, C. Roth, M. Wörle, T. Weyhermüller, G. J. Reiss, U. Schilde, I. Müller, K. Hegetschweiler, *Eur. J. Inorg. Chem.* **2001**, 2525−2542.
[30] A. Blaskó, C. A. Bunton, S. Bunel, C. Ibarra, E. Moraga, *Carbohydr. Res.* **1997**, *298*, 163−172.
[31] J. L. Sudmeier, C. N. Reilley, *Anal. Chem.* **1964**, *36*, 1698−1706.
[32] [32a] J. Springborg, C. E. Olsen, I. Søtofte, *Acta Chem. Scand.* **1995**, *49*, 555−563. [32b] M. Kubiak, T. Glowiak, *Acta Crystallogr., Sect. C* **1986**, *42*, 419−421. [32c] K. M. Doxsee, J. R. Hagadorn, T. J. R. Weakley, *Inorg. Chem.* **1994**, *33*, 2600−2606, and references therein.
[33] [33a] P. D. W. Boyd, M. Gerloch, G. M. Sheldrick, *J. Chem. Soc., Dalton Trans.* **1974**, 1097−1102. [33b] F. A. Cotton, Z. Dori, R. Llusar, W. Schwotzer, *Inorg. Chem.* **1986**, *25*, 3654−3658.
[34] [34a] J. R. Fritch, G. G. Christoph, W. P. Schaefer, *Inorg. Chem.* **1973**, *12*, 2170−2175. [34b] R. M. Hartshorn, S. G. Telfer, *J. Chem. Soc., Dalton Trans.* **2000**, 2801−2808. [34c] F. R. Fronczek, W. P. Schaefer, R. E. Marsh, *Acta Crystallogr., Sect. B* **1974**, *30*, 117−121.
[35] D. Ramprasad, A. G. Gilicinski, T. J. Markley, G. P. Pez, *Inorg. Chem.* **1994**, *33*, 2841−2847.
[36] [36a] W. P. Schaefer, *Inorg. Chem.* **1968**, *7*, 725−731. [36b] N. F. Curtis, W. T. Robinson, D. C. Weatherburn, *Aust. J. Chem.* **1992**, *45*, 1663−1680.
[37] [37a] U. Thewalt, M. Zehnder, S. Fallab, *Helv. Chim. Acta* **1977**, *60*, 867−873. [37b] T. Shibahara, S. Koda, M. Mori, *Bull. Chem. Soc. Jpn.* **1973**, *46*, 2070−2074.
[38] G. J. Gainsford, W. G. Jackson, A. M. Sargeson, *Aust. J. Chem.* **1986**, *39*, 1331−1336.
[39] M. Zehnder, U. Thewalt, S. Fallab, *Helv. Chim. Acta* **1979**, *62*, 2099−2108.
[40] [40a] R. E. Marsh, W. P. Schaefer, *Acta Crystallogr., Sect. B* **1968**, *24*, 246−251. [40b] W. P. Schaefer, S. E. Ealick, D. Finley, R. E. Marsh, *Acta Crystallogr., Sect. B* **1982**, *38*, 2232−2235.
[41] D. D. Dexter, C. N. Sutherby, M. W. Grieb, R. C. Beaumont, *Inorg. Chim. Acta* **1984**, *86*, 19−31.
[42] V. M. Miskowski, B. D. Santarsiero, W. P. Schaefer, G. E. Ansok, H. B. Gray, *Inorg. Chem.* **1984**, *23*, 172−176.
[43] W. P. Schaefer, S. E. Ealick, R. E. Marsh, *Acta Crystallogr., Sect. B* **1981**, *37*, 34−38.
[44] [44a] K. Nakamoto, *Coord. Chem. Rev.* **1990**, *100*, 363−402. [44b] H. A. O. Hill, D. G. Tew, *Compr. Coord. Chem.* **1987**, *2*, 315−333.
[45] A rather small twist angle $\tau = 100.4°$ has been reported for a dinuclear Co^{III}(*tetra*amine)(peroxo) complex with an additional ligating sugar oxygen atom: T. Tanase, T. Onaka, M. Nakagoshi, I. Kinoshita, K. Shibata, M. Doe, J. Fujii, S. Yano, *Inorg. Chem.* **1999**, *38*, 3150−3159.
[46] E. I. Solomon, F. Tuczek, D. E. Root, C. A. Brown, *Chem. Rev.* **1994**, *94*, 827−856.
[47] S. Fallab, M. Zehnder, *Helv. Chim. Acta* **1984**, *67*, 392−398.
[48] S. Fallab, P. R. Mitchell, *Adv. Inorg. Bioinorg. Mech.* **1984**, *3*, 311−377.
[49] F. Tuczek, K. Hegetschweiler, unpublished.
[50] G. A. Lawrance, P. A. Lay, *J. Inorg. Nucl. Chem.* **1979**, *41*, 301−304.
[51] H. Irving, R. J. P. Williams, *Nature* **1948**, *162*, 746−747.
[52] R. D. Hancock, *Acc. Chem. Res.* **1990**, *23*, 253−257.
[53] R. M. Smith, A. E. Martell, R. J. Motekaitis, *Critically Selected Stability Constants of Metal Complexes*, NIST Standard Reference Database 46, version 6.0, Gaithersburg, MD, USA, **2001**.
[54] G. K. Hollingshed, G. A. Lawrance, M. Maeder, M. Rossignoli, *Polyhedron* **1991**, *10*, 409−413.
[55] A. Wojciechowska, L. Bolewski, L. Lomozik, *Monatsh. Chem.* **1991**, *122*, 131−138.

[56] E. Prenesti, P. G. Daniele, M. Prencipe, G. Ostacoli, *Polyhedron* **1999**, *18*, 3233−3241.
[57] In ref.[55] λ_{max} = 575 nm is reported for $[Cu(1,3\text{-diaminopropane})_2]^{2+}$; the estimation according to ref.[56] yields a value of 556±10 nm).
[58] J. Bjerrum, B. V. Agarwala, *Acta Chem. Scand., Ser. A* **1980**, *34*, 475−481.
[59] [59a] P. Comba, T. W. Hambley, G. Lauer, N. Okon, *MOMEC97*, Version 2.1.3. a Molecular Modeling Package for Inorganic Compounds, Heidelberg, **1996**. [59b] P. Comba, T. W. Hambley, *Molecular Modeling of Inorganic Compounds*, 2nd ed., VCH, Weinheim, **2001**.
[60] P. V. Bernhardt, *Inorg. Chem.* **2001**, *40*, 1086−1092.
[61] S. S. Eaton, K. M. More, B. M. Sawant, G. R. Eaton, *J. Am. Chem. Soc.* **1983**, *105*, 6560−6567.
[62] A. Schweiger, G. Jeschke, *Principles of Pulse Electron Paramagnetic Resonance*, Oxford University Press, Oxford, **2001**.
[63] e.g. CuTPP, see: T. G. Brown, B. M. Hoffman, *Mol. Phys.* **1980**, *39*, 1073−1109.
[64] D. T. Richens, A. G. Sykes, *J. Chem. Soc., Dalton Trans.* **1982**, 1621−1624.
[65] L. Fabbrizzi, A. Perotti, A. Profumo, T. Soldi, *Inorg. Chem.* **1986**, *25*, 4256−4259.
[66] A. McAuley, S. Subramanian, T. W. Whitcombe, *J. Chem. Soc., Dalton Trans.* **1993**, 2209−2214.
[67] C. K. Murray, D. W. Margerum, *Inorg. Chem.* **1982**, *21*, 3501−3506.
[68] G. De Santis, L. Fabbrizzi, A. Poggi, A. Taglietti, *Inorg. Chem.* **1994**, *33*, 134−139.
[69] B. de Castro, J. Gomes, M. P. M. Marques, C. F. G. C. Geraldes, *J. Chem. Soc. Dalton Trans.* **1995**, 2041−2044.
[70] A. Ries, K. Hegetschweiler, *NMR-Tit*, Program for the Simulation of pH-Dependent Shifts in NMR Spectra, version 2.0, Saarbrücken, **1999**.
[71] See website http://www.esr.ethz.ch
[72] R. Szosenfogel, D. Goldfarb, *Mol. Phys.* **1998**, *95*, 1295−1308.
[73] P. Gans, A. Sabatini, A. Vacca, *Talanta* **1996**, *43*, 1739−1753.
[74] [74a] R. A. Binstead, B. Jung, A. D. Zuberbühler, *SPECFIT/32*, version 3.0, Spectrum Software Associates, Marlborough, MA 01752, USA, **2000**. [74b] H. Gampp, M. Maeder, C. J. Meyer, A. D. Zuberbühler, *Talanta* **1985**, *32*, 95−101.
[75] CCDC-106171, -106173, and -106611 (excluding structure factors) for **1**Br_2, **2**$Cl_4{\cdot}4H_2O$, and **3**$Cl_2[ZnCl_4][ZnCl_3(H_2O)]{\cdot}H_2O$ contain the supplementary crystallographic data for this paper. These data can be obtained free of charge at www.ccdc.cam.ac.uk/conts/retrieving.html [or from the Cambridge Crystallographic Data Centre, 12 Union Road, Cambridge CB2 1EZ, UK; Fax: (internat.) + 44-1223/336-033; E-mail: deposit@ccdc.cam.ac.uk].
[76] G. M. Sheldrick, *SHELXS-97, Program for Crystal Structure Solution*, Göttingen, **1990**.
[77] G. M. Sheldrick, *SHELXL-97, Program for Crystal Structure Refinement*, Göttingen, **1997**.
[78] H. D. Flack, *Acta Crystallogr., Sect. A* **1983**, *39*, 876−881.

Received October 4, 2002
[I02553]